Revised 12/81

PERMEATION OF ELECTROACTIVE SOLUTES THROUGH ULTRATHIN POLYMERIC FILMS ON ELECTRODE SURFACES

T. Ikeda*, R. Schmehl, P. Denisevich, K. Willman and R. W. Murray*

Kenan Laboratories of Chemistry

University of North Carolina

Chapel Hill, North Carolina 27514

ABSTRACT

The rates of permeation of a series of electroactive solutes, bromide, ferrocene, benzoquinone, diquat, $[Ru(bpy)_2Cl_2]$, $[Fe(bpy)_2(CN)_2]$, and $[Ru(bpy)_2(py)Cl]^+$ have been measured through ultrathin, electrochemically polymerized films like poly-$[Ru(vbpy)_3]^{2+}$. The films are coated on Pt disk electrodes. The permeabilities, expressed as $PD_{S,pol}$, the product of a partition coefficient and a diffusion coefficient in the film, range from very fast (bromide, $> 4 \times 10^{-7}$ cm^2/sec.) to measurable and sensitive to solute size and charge ($2 - 58 \times 10^{-9}$ cm^2/sec.) to immeasurably slow ($[Ru(bpy)_2(py)Cl]^+$, $< 7 \times 10^{-12}$ cm^2/sec.). The permeation rates vary linearly with film thickness; this and the molecular size discrimination rule out transport through larger-than-molecular-dimensional channels and pinholes in the film. The film permeability process is described as membrane diffusion. Relatively pinhole-free films are preparable as thin as 20 - 40 Å.

PERMEATION OF ELECTROACTIVE SOLUTES THROUGH ULTRATHIN POLYMERIC FILMS ON ELECTRODE SURFACES

T. Ikeda*[1], R. Schmehl, P. Denisevich, K. Willman and R. W. Murray*

Kenan Laboratories of Chemistry

University of North Carolina

Chapel Hill, North Carolina 27514

This paper describes electrochemical reactions of acetonitrile solutions of electroactive species at electrodes covered with very thin films (ca. 20 to 450 Å) of redox polymers. Specifically, rates of permeation of electroactive solutes through redox polymer films to the electrode have been measured as a function of film polymeric structure and of solute size and charge. The polymer coated Pt electrodes are prepared by polymerization-inducing reductions of the electroactive monomers[1-5]

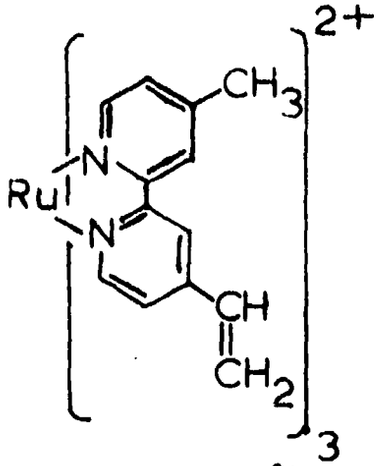

$[Ru(vbpy)_3]^{2+}$

$[Ru(bpy)_2(p\text{-}cinn)_2]^{2+}$

$Ru(bpy)(py\text{-}NHCOCH{=}CHPh)_2^{2+}$

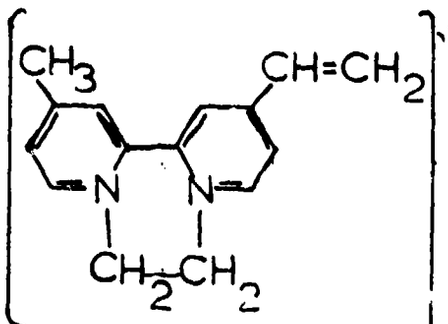

$[VDQ]^{2+}$

[1]Department of Agricultural Chemistry, Kyoto University, Kyoto, Japan

in acetonitrile and are abbreviated Pt/poly-$[Ru(\underline{vbpy})_3]^{2+}$, Pt/poly-$[Ru(\underline{bpy})_2(\underline{p\text{-}cinn})_2]^{2+}$, and Pt/poly-$VDQ^{2+}$, where bpy is 2,2'-bipyridine and p-cinn is N-(4-pyridyl)cinnamide.

The electroactive solutes are p-benzoquinone, ferrocene, diquat (DQ^{2+}; N,N'-ethylene-2,2'-bipyridine), $[Ru(\underline{bpy})_2Cl_2]$, $[Fe(\underline{bpy})_2(CN)_2]$, $[Ru(\underline{bpy})_3]^{2+}$, and $[Ru(\underline{bpy})_2(\underline{py})Cl]^{+}$. Permeabilities of all solutes except $[Ru(\underline{bpy})_3]^{2+}$ were evaluated for the Pt/poly-$[Ru(\underline{vbpy})_3]^{2+}$ films, while for Pt/poly-$[Ru(\underline{bpy})_2)\underline{p\text{-}cinn})_2]^{2+}$, ferrocene and $[Ru(\underline{bpy})_2Cl_2]$ solutions were studied, and for Pt/poly-VDQ^{2+}, solutions of ferrocene, $[Ru(\underline{bpy})_2Cl_2]$, and $[Ru(\underline{bpy})_3]^{2+}$. The solute permeabilities at film coated rotated disk electrodes were determined from the variations of their limiting currents with electrode rotation rate ω and film thickness.

Thorough understanding of solute transport through thin films is important in describing the catalytic or inhibitory behavior of such films. Solute permeation is relevant to processes in ultrathin films, phases, and membranes such as phospholipid bilayer membranes[6], biological cell walls[7], supported oriented-monolayer films[6], drug encapsulation polymers[8], immobilized enzyme systems[9], zeolite particles[10,11], surfactant micellar[12] and vesicle[13,14] structures, and corrosion-inhibiting films on metals, electronic microcircuits, and semiconductor electrodes. The actual transport constants are in most cases, however, unmeasured, one difficulty being that of preparing ultrathin films in suitable physical forms and another being that of distinguishing transport as a solute "dissolved" in the film (which we shall term membrane diffusion) from transport through film imperfections (pinhole and channel diffusion).

Transport of solutes through redox polymer coated electrodes is important in their applications to electrocatalysis[15-39] and photoelectrochemistry[40-43] and in relation to the transport of electrochemical charge through such polymers which occurs via electron self-exchange

reactions of the redox sites[22,39,41,44-52]. Film permeability is of particular interest with respect to the evolving theory[32-39,44] of mediated electrocatalysis. Again, the transport data available[17,19,21] to address these problems quantitatively are very limited, and there has been no study of the variation of permeability with either solute or film structure.

Our experiences with electrochemically prepared redox polymer films as used in bilayer film electrodes[1,2] suggest that these films are often free of imperfections even when the film contains only 5-10 layers of redox monomer sites. It is furthermore possible to systematically vary the thickness d of these films as measured in mol./cm^2, Γ_T, of ruthenium (III/II) and $VDQ^{2+/1+}$ redox sites. Γ_T is determined from voltammetry of the film in monomer free solution. The films thus represent an opportunity to address the difficult issue[17] of film imperfections and to systematically examine structural effects on ultrathin film transport.

EXPERIMENTAL

Electrochemical Polymerization of Redox Polymer Films on Electrodes. Synthesis of the electroactive monomers $[Ru(\underline{vbpy})_3]^{2+}$, $[Ru(\underline{bpy})_2(\underline{p\text{-}cinn})_2]^{2+}$, and VDQ^{2+}, details of their reductions to form polymer films on electrodes, electrochemical properties of the films and the kinetics of their electron transfer mediation reactions with several electroactive solutes are described elsewhere[3-5,33,53]. Briefly, to prepare a film, the potential applied to a Teflon-shrouded Pt disk electrode is swept repeatedly between 0 V vs. SSCE and the second of the one-electron monomer reduction waves in 0.1, 0.5, and 1 mM thor-

oughly-degassed acetonitrile solutions of the three monomers, respectively. The thickness of the polymer films built up in this manner increases linearly with the number of repetitive potential sweeps[3], as assessed by the increasing peak currents for the two reduction waves of still-electroactive, polymerized monomer, and more quantitatively by the charge under slow potential scan cyclic voltammetric waves for the $Ru^{III/II}$ and $VDQ^{2+/1+}$ couple waves in monomer free acetonitrile solution. Permeability results include data for electrodes prepared as a group and bearing a series of film thicknesses, as well as data from individual electrodes prepared over a period of several months. Following film deposition, electrodes were thoroughly rinsed with acetonitrile and carefully stored in air in a closed vial. To minimize the incidence of film imperfections caused by handling, films were ordinarily not employed for more than one or two sets of permeability measurements with an electroactive solute.

The Pt/poly-$[Ru(\underline{vbpy})^{2+}$/PVFer bilayer electrode was prepared as described elsewhere[1,2], by evaporation of a droplet of polyvinylferrocene in toluene solution on the surface of a Pt/poly-$[Ru(\underline{vbpy})_3]^{2+}$ electrode.

Procedure for Permeability Measurement. Permeability measurements were based on the limiting currents of voltammograms of the electrochemical oxidations or reductions of the electroactive solutes at polymer film coated Pt disk electrodes rotated in Pine Instrument Co. Mpdel PIR and NSY assemblies varying electrode rotation rate over 400-10^4 rpm ($\omega^{1/2}$ = 20 - 100 $rpm^{1/2}$). Voltammograms for the ruthenium polymer films were extended to include the electron transfer mediated wave for the solute which occurs near the $Ru^{III/II}$ potential (vide infra). The acetonitrile

solutions were 0.1 M in Et_4NClO_4 supporting electrolyte, and usually < 0.5 mM in electroactive solute. The low solute concentration was chosen to avoid alterations in film swelling, and in the electron transfer mediated wave, to avoid charge transport rate limitations in the polymer films[53].

Electrochemical Equipment and Chemicals. $[Ru(bpy)_2Cl_2]$ and $[Fe(bpy)_2(CN)_2]$ were synthesized by literature procedures[54,55]; ferrocene (Aldrich) was used as received, and p-benzoquinone (J. T. Baker) after sublimation. Electrochemical equipment and cells were conventional. All potentials are referenced against a NaCl-saturated SCE, designated SSCE.

RESULTS AND DISCUSSION

Membrane Diffusion Theory for Rotated Disk Electrode. The limiting current i_ℓ for electrochemical reaction of a solute which partitions into (with coefficient P) and diffuses to a rotated disk electrode through a membrane barrier with diffusion constant $D_{S,pol}$ (different from that in the solution D_S) is described by the equation[56]

$$\frac{1}{i_\ell} = \frac{1}{nFAD_{S,pol}PC_S/d} + \frac{1}{0.62nFAD_S^{2/3}\nu^{-1/6}\omega^{1/2}C_S} \qquad (1)$$

where d is membrane thickness and ω is in rad./sec. The two terms on the right hand side of equation 1 represent respectively the rates of solute diffusion through the membrane and through the Levich depletion layer in solution. If $D_S^{2/3}\nu^{-1/6}\omega^{1/2} \ll PD_{S,pol}/d$ (e.g., very thin film or large $PD_{S,pol}$), the diffusion through the Levich layer is the slower of the two and a ("Levich")

plot of i_ℓ vs. $\omega^{1/2}$ is linear with zero intercept. If diffusion through the membrane is slower, the Levich plot is not linear, but a plot of i_ℓ vs. $\omega^{-1/2}$ (an "inverse Levich plot"), is and $PD_{S,pol}/d$ can be evaluated from its intercept.

Important features of an inverse Levich plot are: (i) its slope should yield the same D_S as observed at a naked rotated Pt disk electrode, independent of C_S or d , (ii) the intercept should be inversely proportional to C_S , and (iii) the intercept should be proportional to d (and accordingly Γ_T for the redox polymer films). The latter, vital criterion has not been satisfactorily examined for membrane coated rotated disks.

We should note that membrane diffusion is only one of four conceivable modes of reaction of an electroactive solute at a polymer film coated electrode. The other three are[17]: (a) electronic conductivity of the film leading to electrolysis of the solute at the film/solution interface, (b) oxidation or reduction of the solute by electron transfer mediation by redox sites in the polymer film, and (c) diffusion of the electroactive solute through the solvent in film imperfections (channels and pinholes with dimensions much larger than that of the solute or of monomer sites in the film). Experimental results ruling out these three alternative processes will be identified as we come to them.

Poly-$[Ru(vbpy)_3]^{2+}$ and poly-$[Ru(bpy)_2(p\text{-}cinn)_2]^{2+}$ films. Electroreductive polymerization of vinyl monomers like $[Ru(vbpy)_3]^{2+}$ in acetonitrile produces[3] an adherent, intractably insoluble polymeric film of the complex on the electrode surface which undergoes electron transfer reactions at potentials similar to those of the monomer, Figure 1, Curve

A. The polymerization is rationalized by the thesis[1,3] that the metal complex reductions are ligand localized, and that radical ions of such activated olefins are prone to coupling and polymer-forming reactions. In an investigation into the generality of this chemistry we have established[4] that one and (more rapidly) two electron reductions of the monomer $[Ru(\underline{bpy})_2(\underline{p\text{-}cinn})_2]^{2+}$ also produce stable, adherent redox polymer films which are electroactive as shown in Figure 1, Curve B.

Spectroelectrochemical experiments show[2] that the electrochemical charge under a slow potential scan poly-$[Ru(vbpy)_3]^{3+/2+}$ cyclic voltammogram, Figure 1, Curve A, measures all of the film's redox sites, Γ_T, mol./cm^2. Over the range $\Gamma_T = 10^{-10}$ to 10^{-8} mol./cm^2, the poly-$[Ru(vbpy)_3]^{2+}$ and poly-$[Ru(bpy)_2(p\text{-}cinn)_2]^{2+}$ voltammetric waveshapes remain constant, which implies[53] that activity parameter G and correspondingly the density of the charge redox sites do not vary substantially over this range. Accordingly, we assume here that the physical thicknesses of the poly-$[Ru(\underline{vbpy})_3]^{2+}$ and poly-$[Ru(\underline{bpy})_2(\underline{p\text{-}cinn})_2]^{2+}$ films are proportional to Γ_T. Densities of bulk samples of poly-$[Ru(\underline{vbpy})_3]^{2+}$ and poly-$[Ru(\underline{bpy})_2(\underline{p\text{-}cinn})_2]^{2+}$ are 1.35 and 1.4 g/cm^3, which correspond to concentrations of ruthenium redox sites in the polymer of $C_{Ru} = 1.5 \times 10^{-3}$ and $C_{Ru}' = 1.2 \times 10^{-3}$ mol./cm^3, respectively. Film thicknesses estimated by $d = \Gamma_T/C_{Ru}$ and $d = \Gamma_T/C_{Ru}'$ assume that the ultrathin polymer films swell to the same extent in acetonitrile and the solvents used for the density (flotation) measurement. To avoid this assumption in comparison of equation 1 to film thickness, the membrane permeability results will be expressed as

$$\Gamma_T(PD_{S,pol}/d) = PD_{S,pol}C_{Ru} \qquad (2)$$

which contains no assumptions about film density.

From substantial differences in polymer film forming rates with the degree of vinyl substituion of otherwise similar complexes (e.g., $[Ru(\underline{vbpy})_3]^{2+}$ *vs.* $[Ru(\underline{bpy})_2(\underline{vbpy})]^{2+}$) which seem best interpreted in steric terms, and from other data, we believe that coupling reactions of sterically bulky vinyl-bipyridine radical anion sites are often terminated at the dimer stage. The poly-$[Ru(\underline{vbpy})_3]^{2+}$ polymer thereby contains not only *chain* polymer segments but also elements of a three-dimensional matrix of metal complexes joined by bridging-$(\underline{bpy})(CH_2)_4(\underline{bpy})$- ligands. Analogously, poly-$[Ru(\underline{bpy})_2(\underline{p\text{-}cinn})_2]^{2+}$ would contain bridging structures like

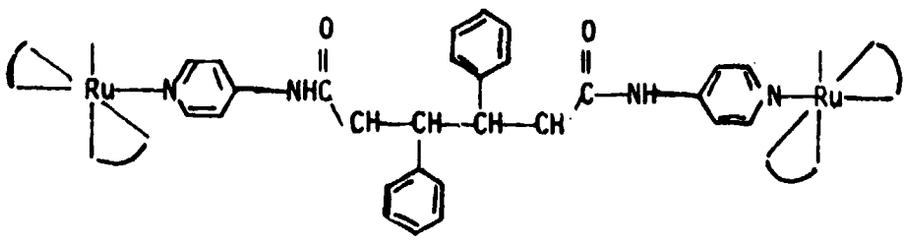

(3)

where the vinyl coupling reaction is depicted as "tail-to-tail" as expected from studies of hydrodimerization of radical anions of activated olefins[57]. Because of the longer spacing between the perimeters of the bipyridine ligands in equation 3, and because poly-$[Ru(\underline{bpy})_2(\underline{p\text{-}cinn})_2]^{2+}$ should be less highly three-dimensionally cross-linked, we anticipated that the poly-$[Ru(\underline{bpy})_2(\underline{p\text{-}cinn})_2]^{2+}$ polymer film would be more permeable to electroactive solutes, which was borne out by the experimental results, below.

Three classes of solute behavior were observed at these films: very fast, very slow, and measureable permeation. These and their eq. 1 characteristics are outlined in Table I.

Fast Permeation Through poly-$[Ru(vbpy)_3]^{2+}$ Film. A voltammogram in tetraalkylammonium bromide at a rotated Pt/poly-$[Ru(vbpy)_3]^{2+}$ electrode is shown in Figure 2, Curve B. The rising part of the bromide → bromine wave has an electrochemically irreversible shape; its gently sloping wave plateau has superimposed upon it the film electrode poly-$[Ru(vbpy)_3]^{3+/2+}$

cyclic voltammogram which is shown in Curve A at the same electrode rotation rate in bromide-free solution. Limiting currents for the bromide/bromine reaction measured at +0.95 volt. vs. SSCE follow the Levich equation (Figure 2 inset, proportional to $\omega^{1/2}$, i.e., the right-hand term of eq. 1 is dominant). Further, the shape of a bromide oxidation voltammogram at a naked rotated Pt disk[58a] is identical to Figure 2, Curve B, at all potentials more negative than +0.95 volt, and its limiting currents (at +0.95 volt) fall exactly on those in the Figure 2 inset.

These results demonstrate that bromide permeation through poly-$[Ru(\underline{vbpy})_3]^{2+}$ to react at the Pt surface is too fast to measure at our accessible electrode rotation rates, for the film thicknesses employed, up to 3.6×10^{-9} mol./cm^2 or ca. 210 Å. Assuming that a 10% deviation from the Levich plot (Figure 2 inset) could have been detected at the highest electrode rotation rate, we estimate that $PD_{S,pol}/d \geq 0.17$, or $PD_{S,pol}C_{Ru} \geq 6.0 \times 10^{-10}$ for bromide permeation. Rotated electrodes coated with much thicker films of poly-$[Ru(\underline{vbpy})_3]^{2+}$ would be necessary to further define the bromide permeability. The high bromide permeability is relevant to understanding charge transport rates through poly-$[Ru(\underline{vbpy})_3]^{2+}$ films as further discussed below.

Very Slow Permeation Through poly-$[Ru(\underline{vbpy})_3]^{2+}$ Film. At naked Pt, an acetonitrile solution of $Ru(bpy)_2(py)Cl^+$ gives a reversible (slope 60 mV.) voltammetric wave, Figure 3, Curve A, with well-defined limiting currents which obey the Levich equation (inset, – x –). At Pt/poly-$[Ru(\underline{vbpy})_3]^{2+}$, this complex gives a similarly formed voltammogram with superimposed poly-$[Ru(\underline{vbpy})_3]^{3+/2+}$ electrode film reaction as shown in Figure 3, Curve B. However, in contrast to the bromide reaction, the

naked and coated electrode reactions occur at different potentials; the rising part of Figure 3, Curve B, is shifted by +140 mV relative to the naked electrode result (Curve A). The foot of the voltammogram at the polymer coated electrode at potentials where currents on the naked electrode are quite large, shows no hint of an attenuated facsimile of the naked electrode voltammogram (see enlargement, Figure 3).

These results can be interpreted in terms of very slow permeation of $[Ru(\underline{bpy})_2(\underline{py})Cl]^+$ into the poly-$Ru(vbpy)_3^{2+}$ film so that the complex is not oxidized in significant quantity at the Pt/film interface, but is instead oxidized indirectly by Ru^{3+} sites near or at the film/solution interface:

$$[Ru(\underline{bpy})_2(\underline{py})Cl]^+ + Pt/poly\text{-}[Ru(\underline{vbpy})_3]^{3+} \longrightarrow [Ru(\underline{bpy})_2(\underline{py})Cl]^{2+} + Pt/poly\text{-}[Ru(\underline{vbpy})_3]^{2+} \quad (4)$$

Reaction 4 has a large driving force (ΔE° = 375 mV.) and by comparison to mediation of the oxidation of other ruthenium complexes (e.g., $[Ru(\underline{bpy})_3]^{2+}$) with smaller ΔE° but large electron transfer cross-reaction rates[33], can be expected to be quite fast. Limiting currents for Curve B accordingly obey the Levich equation, see Figure 3 inset – o – , showing that mass transfer of $[Ru(\underline{bpy})_2(\underline{py})Cl]^+$ limits the current, not the rate of Reaction 4. Additionally, $E_{1/2}$ for Curve B is considerably more negative than E°_{surf} for poly-$[Ru(\underline{vbpy})_3]^{3+/2+}$, another manifestation of fast electron transfer as discussed in another paper[53].

Assuming that a voltammetric wave 1% of Curve A, Figure 3, could have been detected at the foot of Curve B (but was not), we estimate that $PD_{S,pol}/d \leq 2.0 \times 10^{-4}$ or $PD_{S,pol}C_{Ru} \leq 1.6 \times 10^{-13}$ for $[Ru(\underline{bpy})_2(\underline{py})Cl]^+$. The same results were obtained in four experiments, where the

concentration of $[Ru(bpy)_2(py)Cl]^+$ was varied from 0.1 - 0.2 mM and the film coverages were 7.2, 7.8, 11.0, and 25.0 x 10^{-10} mol./cm^2 for a film thickness range of ca. 42 - 147 Å.

Measurable Permeation Rates Through poly-$[Ru(vbpy)_3]^{2+}$. Ferrocene is oxidized in two waves at a rotated Pt/poly$[Ru(vbpy)_3]^{2+}$ disk electrode (Figure 4, Curves A-D). The first wave ($E^{\circ\prime}$ = +0.38 volt vs. SSCE) lies at the same potential as the naked electrode reaction (Curve E) and has limiting currents (measured at 0.6 volt) which are not proportional to $\omega^{1/2}$ (inset, -x-), but which clearly fit the membrane diffusion equation 1 by giving a linear $1/i_\ell$ vs. $\omega^{-1/2}$ plot (Figure 5, Curve A). Similar results were obtained in five additional experiments on electrodes with different poly-$[Ru(vbpy)_3]^{2+}$ film thicknesses Γ_T and at different ferrocene concentrations C_S, as illustrated by the linear reciprocal Levich plots of Figure 5, Curves B and C. These data further confirm the membrane diffusion model. First, slopes of the $1/i_\ell$ vs. $\omega^{-1/2}$ plot are inversely proportional to C_S (compare Figure 5, Curves A vs. B) and independent of Γ_T (e.g., film thickness, compare Curves B and C). This evidence is summarized in Table II by the constancy of D_S, the diffusion coefficient for ferrocene in acetonitrile as calculated from eq. 1, and by agreement of this value with D_S observed at a rotated naked Pt electrode (2.3 x 10^{-5} cm^2/sec.) and literature values[59]. Secondly, the intercepts (Table II) of the inverse Levich plots are, within the data error limits, inversely proportional to both Γ_T and C_S, the former over nearly a ten-fold range, as shown by constancy of the intercept-derived product $PD_{S,pol}C_{Ru}$ in TableII. Thirdly, as expected from eq. 1, at sufficiently large film thicknesses (the examples with Γ_T = 2.5 x 10^{-9} and 6.8 x 10^{-9} mol./cm^2),

transport through the polymer film is so slow that the limiting current for the (first) ferrocene oxidation wave becomes essentially independent of the electrode rotation rate.

The second ferrocene oxidation wave in Figure 4, Curves A-D at E ~ +0.85 V is due to the rapid poly-$[Ru(\underline{vbpy})_3]^{3+}$ electron transfer mediated reaction

$$Fer + Pt/poly\text{-}[Ru(\underline{vbpy})_3]^{3+} \rightarrow Fer^{+} + Pt/poly\text{-}[Ru(\underline{vbpy})_3]^{2+} \qquad (5)$$

which occurs on the leading edge of the poly-$[Ru(\underline{vbpy})_3]^{3+/2+}$ wave (dashed curves) in the same manner as Rxn. 4 for $[Ru(\underline{bpy})_2(py)Cl]^{+}$ discussed above. The appearance of the second wave supports interpretation of the first wave as representing membrane diffusion as opposed to electron transfer mediation. Reaction 5 is very fast, so that diffusion of ferrocene in the solution limits the current; the limiting current measured at 1.1 volt follows the Levich equation as shown by Figure 4, (—o—). This particular experimental situation appears not to have been previously described.

Analogous experiments were conducted for the solutes p-benzoquinone, $diquat^{2+}$, $[Ru(\underline{bpy})_2Cl_2]$, and $[Fe(\underline{bpy})_2(CN)_2]$. The slow membrane diffusion and small limiting currents for direct oxidation of the latter two complexes diffusing through the polymer film to the Pt/film interface are illustrated by Figure 6, Curve B for $[Ru(\underline{bpy})_2Cl_2]$. Curve A of Figure 6 corresponds to the $[Ru(\underline{bpy})_2Cl_2]^{+1/0}$ reaction at naked Pt (limiting currents follow the Levich relationship, Figure 6 insert —x—). Even with very thin poly-$[Ru(\underline{vbpy})_3]^{2+}$, $\Gamma_T = 7.8 \times 10^{-10}$ mol./cm^2, or ca. 46 Å, the currents from Curve B are nearly independent of ω (Figure inset —●—)

and give $1/i_\ell$ *vs.* $\omega^{-1/2}$ plots according to eq. 1. Results at different C_S (constant D_S from slope) and Γ_T (constant $PD_{S,pol}C_{Ru}$ from the intercept), Table II, again support adherence to the membrane diffusion theory, eq. 1. The voltammograms and numerical data for $[Fe(\underline{bpy})_2(CN)_2]$ are similar. The data scatter in $PD_{S,pol}C_{Ru}$ is larger than that for ferrocene owing to the small slopes of the reciprocal Levich plots and to the small measured limiting currents, but general adherence to the membrane relation is obvious.

Like ferrocene, a second (rapid electron transfer mediated) wave is observed for $[Ru(\underline{bpy})_2Cl_2]$ and $[Fe(\underline{bpy})_2(CN)_2]$, the overall limiting current (—o—) of which is, like that at naked Pt (—x—), proportional to $\omega^{1/2}$ (Figure 6 inset) and controlled by diffusion of the complex in the solution.

p-benzoquinone and diquat reductions occur in two one-electron waves on naked Pt; the first wave for each is sufficiently positive of the poly-$[Ru(\underline{vbpy})_3]^{2+/1+}$ reaction that electron transfer mediation of the reduction isn't expected. The permeation wave for diquat^{2+} occurs (Figure 7, Curve B) at the same potential as diquat^{2+} reduction on naked Pt (Curve A), and gives linear reciprocal Levich plots (Figure 7 inset). D_S and $PD_{S,pol}C_{Ru}$ results for diquat^{2+}, and for benzoquinone, are given in Table II.

Average $PD_{S,pol}C_{Ru}$ values in Table II display interesting and systematic variations which are discussed later.

Measurable Permeation Rates Through poly-$[Ru(bpy)_2(p\text{-}cinn)_2]^{2+}$. Voltammetry of $[Ru(\underline{bpy})_2Cl_2]$ and of ferrocene solutions at rotated poly-$[Ru(\underline{bpy})_2(\underline{p\text{-}cinn})_2]^{2+}$ disk electrodes is very similar to that in Figures 4-6, and $1/i_\ell$ *vs.* $1/\omega^{1/2}$ plots are linear with intercepts inversely propor-

tional to Γ_T . Results for $[Ru(\underline{bpy})_2Cl_2]$ and ferrocene permeation into poly-$[Ru(\underline{bpy})_2(\underline{p\text{-}cinn})_2]^{2+}$, where C'_{Ru} is the concentration of redox sites (Table III),are both about six times larger than $PD_{S,pol}C_{Ru}$ for $[Ru(\underline{bpy})_2Cl_2]$ and ferrocene in poly-$[Ru(\underline{vbpy})_3]^{2+}$ (Table II). The striking permeability differences between the two solutes in each film and between the two films are illustrated in Figure 8. Expressed as $PD_{S,pol}C$, the poly-$[Ru(\underline{bpy})_2(\underline{p\text{-}cinn})_2]^{2+}$ film is more permeable.

Permeation Rates Through poly-Vinyldiquat^{2+}. In electrochemical polymerization of the vinyldiquat monomer (VDQ^{2+}), the film thickness as with the ruthenium complex polymers, is controlled by the period of reduction, monomer concentration, and mass transfer mode, and is measured in terms of the coverage of electroactive diquat sites, Γ_T mol./cm^2, from the charge under slow potential sweep cyclic voltammograms of the film's poly-$VDQ^{2+/+}$ reaction. The Pt/poly-VDQ^{2+} film, formed from a sterically smaller, monovinyl species, is expected to be a linear chain, polycationic polymer[5].

Ferrocene is oxidized at a rotated Pt/poly-VDQ^{2+} disk electrode (Figure 9, Curve B) at the same potential as on naked Pt (Curve A), but with much smaller limiting current. Limiting currents (measured at +0.6 V) give linear reciprocal Levich plots the intercepts of which lead to constant $PD_{S,pol}C_{VDQ}$ values (Table IV) over a three-fold range of Γ_T . Permeation of $[Ru(\underline{bpy})_2Cl_2]$ and of $[Ru(\underline{bpy})_3]^{2+}$ through the same $\Gamma_T = 1.3 \times 10^{-9}$ mol/cm^2 Pt/poly-VDQ^{2+} electrode employed in the ferrocene experiments gave very small, nearly rotation rate-independent limiting currents for oxidation of the complexes; their $PD_{S,pol}C_{VDQ}$ values are lower than those for ferrocene (Table IV).

Permeabilities for ferrocene through the thinnest poly-VDQ^{2+} films are difficult to reproduce. For instance, a film specimen with coverage

$\Gamma_T \sim 2 \times 10^{-10}$ mol./cm^2 gave a much larger permeability than that in Table IV, presumably because of a high incidence of pinholes at this extreme thinness. Since a poly-VDQ^{2+} film with $\Gamma_T = 4.4 \times 10^{-10}$ mol./cm^2 corresponds (assuming unit film density or $C_{VDQ} = 2.4$ M) to an average ca. 19 Å thickness, it is understandable that it is technically difficult to avoid pinholes. That the still very thin $\Gamma_T = 4.4 \times 10^{-10}$ mol./cm^2 film was successfully made and shows a modest permeability which is the same as that of a film three times as thick is itself rather remarkable.

Figure 9 shows also cyclic voltammetry of ferrocene at stationary naked Pt and Pt/poly-VDQ^{2+} electrodes. The classically shaped naked electrode wave (Curve C) is altered to a shape (Curve D) similar to a "CE mechanism" voltammogram[60], where the electrochemical reaction is preceded by a kinetically slow reaction. In Curve D, the slow step is the membrane diffusion process. Permeabilities could in principle be evaluated from studying Curve D as a function of potential sweep rate, but the rotated disk approach is based on a simpler theoretical formulation.

Comparison of Permeabilities. Experimental results for $PD_{S,pol}C$ (Tables II - IV) are converted in Table V to $PD_{S,pol}$ based on $C_{Ru} = 1.5 \times 10^{-3}$, $C'_{Ru} = 1.3 \times 10^{-3}$, and $C_{VDQ} = 2.4 \times 10^{-3}$ mol./cm^3. Given the general insolubility and cross-linked nature (of the ruthenium polymers), the swelling errors in these redox site concentrations are probably less than 2X. Even at a presumed 2X uncertainty in the derived $PD_{S,pol}$, substantial structural effects are apparent. The Table V values appear to systematicaly and sensitively reflect the size and charge of the electroactive solute and the polymer membrane structure.

For poly-$[Ru(\underline{vbpy})_3]^{2+}$ films, the $PD_{S,pol}$ values vary over a $> 10^4$ range. Molecular diameters of the neutral solutes increase and solute permeabilities, $PD_{S,pol}$, through the poly-$[Ru(\underline{vbpy})_3]^{2+}$ polymer films decrease in the order: p-benzoquinone, ferrocene, $[Ru(\underline{bpy})_2Cl_2]$, $[Fe(bpy)_2(CN)_2]$. The differences between $[Ru(bpy)_2Cl_2]$, (o) and ferrocene (x) permeabilities is illustrated from the slope differences in Figure 8. Such a fine grained molecula size discrimination is not at all expected if the neutral electroactive solutes primarily diffuse to the Pt electrode through generally dispersed polymer structure imperfections (e.g., pinholes and large channels) with dimensions large compared to molecular monomers. Also, such a > 100X range of permeabilities is not consistent with reaction via an electronic conduction mechanism. The permeability ordering clearly demonstrates that transport occurs mainly through spaces in the film structure which have dimensions near those of the solutes. In this sense we agree with the description of Peerce and Bard[17] of a quite different polymer, that the film can be regarded as a viscous, concentrated poly-electrolyte solution into which the electroactive solute "dissolves" and diffuses.

Films of poly-$[Ru(\underline{bpy})_2(\underline{p\text{-}cinn})_2]^{2+}$ involve longer chains bridging adjacent ruthenium sites, should also be less highly cross-linked, and are correspondingly more permeable to neutral solute than poly-$[Ru(\underline{vbpy})_3]^{2+}$, Figure 8.

Positive charge on the electroactive solute depresses its membrane diffusion rate through the poly-cationic films. The effect in poly-$[Ru(\underline{vbpy})_3]^{2+}$ is ca. 10X, comparing ferrocene with $diquat^{2+}$ and $[Ru(\underline{bpy})_2Cl_2]$ with $[Ru(\underline{bpy})_2(\underline{py})Cl]^+$. Although we have no evidential basis for separating the $PD_{S,pol}$ product it seems reasonable to assign this difference to a less than unity partition coefficient, $\underline{P}$. Ion association in the films is probably extensive, otherwise the electrostatic cation exclusion would yield an even larger diminution in P.

In this connection, we should note that it is already evident that small cations like Li^+ and Et_4N^+ can penetrate poly-$[Ru(\underline{vbpy})_3]^{2+}$ films, observing[3] that the film's ohmic resistance is lowered by increasing the external concentrations of $LiClO_4$ and Et_4NClO_4 supporting electrolytes.

Permeabilities in the poly-VDQ^{2+} film also follow variations in solute molecular size and charge, but the data there are much less extensive. From the ferrocene data, based on a series of Γ_T, the poly-VDQ^{2+} polymer is less permeable than poly-$[Ru(\underline{vbpy})_3]^{2+}$.

The relative pinhole-freeness of the electrochemically polymerized films deserves comment, since demonstrably pinhole-free films with sub-100 Å dimensions are uncommon. We suspect that the dimensional perfection of the films is aided by current density variations during electrochemical reduction of dissolved monomer. Consider that in a film of poly-$[Ru(\underline{vbpy})_3]^{2+}$ in the early stages of its formation (a short period of monomer reduction), the current <u>density</u> for further reduction of monomer rises at any large holes and gaps in the film since the resistance to ion flow, in the solution present in those gaps, is less than that in the film[61]. Polymer growth is thereby promoted at the pinhole, tending to eliminate it, e.g., a <u>self-sealing process</u>. This characteristic of electrochemically formed polymer films is not unique to the poly-$[Ru(\underline{vbpy})_3]^{2+}$ materials, since electrode passivation during monomer oxidation[62] is a well-known phenomenon. The poly-$[Ru(\underline{vbpy})_3]^{2+}$ films differ, however, by continuing to grow following sealing of pinholes owing to their ability to transport electrochemical charge to the polymer/solution boundary[63], where film growth continues.

<u>Permeability and Film Thickness</u>. The clear proportionality of the intercepts of $1/i_\ell$ <u>vs.</u> $\omega^{-1/2}$ plots to film thickness as established by

Γ_T is an additional key element in excluding pinhole or channel phenomena in favor of the membrane diffusion model. Theory by Landsberg[64-67] for reactions of solutes at active sites on rotated disks (equivalent to reactions through pinholes in a film) indicates that for the limiting condition, diffusion layer in the solution $\delta \gg$ spacing and diameter of active site, a plot of i_ℓ^{-1} vs. $1/\omega^{1/2}$ would be linear with slope inversely proportional[68] to the overall, projected electrode area ($\gg$ active site area) and intercept a function of the ratio of pinhole diameter and spacing. To accomodate the observed experimental behavior of the reciprocal Levich plot intercepts with this pinhole theory, the variation of the pinhole diameter/spacing ratio would have to fortuitously mimic a linear Γ_T-intercept relation. The effect would furthermore have to be reproducible over a series of electrode specimens and accurately repeated for three different polymer film structures. We believe this is a highly implausible scenario for the data in Tables II - IV. Most importantly, we draw attention again to the observed, large variations in the intercept values with solute size, as discussed above, which is inconsistent with transport through pinholes of much greater than molecular diameters.

Reciprocal Levich plot intercept-Γ_T proportionality is also important with regard to the average distance over which electrons are transferred between the Pt surface and electroactive solutes diffusing in the membrane. If the electron transfer distance were an appreciable fraction of the film thickness, then the intercept-Γ_T proportionality (at large Γ_T) would change to an exponential relation at small Γ_T, since distance-related barriers to electron transfer are exponential in form. While slight increases in $PD_{S,pol}C_{Ru}$ are observed at low Γ_T studies for several solutes in poly-$[Ru(\underline{vbpy})_3]^{2+}$, this is not generally

the case as shown in Figure 8. It is possible that fluctuations in the data at low Γ_T are due to a higher incidence of film imperfections. The thinnest films in which the Γ_T-intercept proportionality was successfully maintained are 4.1×10^{-10} mol./cm^2 poly-[Ru(bpy)$_2$(p-cinn)$_2$]$^{2+}$ (ca. 34 Å based on $C'_{Ru} = 1.2 \times 10^{-3}$) and 4.4×10^{-10} mol./cm^2 poly-VDQ^{2+} (ca. 18 Å based on $C_{VDQ} = 2.4 \times 10^{-3}$).

Thirdly, the intercept-Γ_T proportionality indicates that topological roughness (depth of valleys and mountains) of the film is not a significant fraction of film thickness for poly-[Ru(vbpy)$_3$]$^{2+}$. This assertion that the microscopic roughness of the film is minimal is consistent with Γ_T-independent mediation rates $k_{crs}\Gamma$ for electron transfer reaction of the films with substrate-solutes in the solution[33,53] where Γ is the reacting quantity of redox sites at the film/solution interface.

Finally, the measured permeabilities of $PD_{S,pol}$ in Table V can be used to estimate the average depth of permeation of an electron transfer-mediated substrate into the redox polymer film before being consumed by reaction with a mediator site. Rxn. 4 (Figure 3B) and rxn. 5 (Figure 4, second wave) are examples of such reactions. From eq. 10 in the theoretical treatment of electrocatalysis by Saveant[39], the ratio of permeability and mediation rates $PD_{S,pol}/k_{crs}\Gamma$ is equal to the average penetration depth. From this, penetration depths for the mediated substrates in Rxns. 4 and 5 are estimated[69] as ca. 10^{-3} and 2.6 Å, respectively. These trivially small distances support our view[33,53] that electron transfer may actually occur without significant penetration of the substrate into the film; i.e., the redox polymer surface acts as the "electrode surface". This then is the $\kappa = 0$ case of the Saveant treatment[39].

Bromide Permeability and Charge Transport. The high permeability of poly-$[Ru(\underline{vbpy})_3]^{2+}$ films to bromide ions is a significant clue in understanding charge transport through them. Charge transport through poly-$[Ru(\underline{vbpy})_3]^{2+}$ refers to migration of electrons to/from the Pt electrode by electron self-exchange[2,3] between neighbor redox sites, e.g.,

$$\sim[Ru(\underline{vbpy})_3]^{3+} + \sim[Ru(\underline{vbpy})_3]^{2+} \rightarrow \sim[Ru(\underline{vbpy})_3]^{2+} + \sim[Ru(\underline{vbpy})_3]^{3+} \quad (6)$$

Migration of electrochemical charge in this manner is phenomenologically equivalent to diffusion and its rate can be measured[48] as a diffusion constant D_{ct}. We have measured[3] D_{ct} in poly-$[Ru(\underline{vbpy})_3]^{2+}$ films by several procedures and, assuming $C_{Ru} = 1.5$ M, $D_{ct} = 1.8 \times 10^{-10}$ cm^2/sec.

The molecular interpretation of charge transport diffusion constants has been the object of much discussion[22,32,39,44-52,58b] but few explicit experimental insights exist into choices between control of D_{ct} by the barrier to the electron hopping event, by the internal mobility

(self-diffusion) of redox polymer sites, or by barriers to the motion of counterions. In reaction 6, transfer of the electron must be accompanied by motion of a charge compensating perchlorate ion. If we presume (reasonably) that perchlorate and bromide ions have similar mobilities in poly-$[Ru(\underline{vbpy})_3]^{2+}$ films, then the rate o migration of perchlorate in this film occurs (like bromide) at a rate $PD_{S,pol} > 3 \times 10^{-7}$ cm^2/sec (Table V). This exceeds by $> 10^3X$ the rate of migration of electrons by reaction 6, $D_{ct} = 1.8 \times 10^{-10}$ cm^2/sec. The strong inference to be drawn from this comparison is that, for this particular redox polymer, the rate of electrochemical charge migration is <u>not</u> controlled by the rate of migration of ClO_4^- counterions, since the latter have, by analogy to bromide ions, a much higher mobility.

<u>Redox Polymer Bilayer Films</u>. We have recently described[1,2] electrodes coated with <u>two</u> layers of redox polymers (e.g., bilayer films). The assembly Pt/poly-$[Ru(\underline{vbpy})_3]^{2+}$/poly(vinylferrocene) is an example. The PVFer is spatially isolated from the Pt surface by the poly-$[Ru(\underline{vbpy})_3]^{2+}$ film, forcing its oxidation reaction to occur near the electrode potential for Ru(III) production, by the mediation reaction.

$$\text{poly-}[Ru(\underline{vbpy})_3]^{3+} + PVFer \rightarrow \text{poly-}[Ru(vbpy)_3]^{2+} + PVFer^+ \qquad (7)$$

which is called a (ferrocenium) charge <u>trapping</u> reaction.

The trapped $PVFer^+$ state is stable for considerable periods when the poly-$Ru(vbpy)_3^{2+}$ inner film layer is reasonably thick. We were interested in how <u>thin</u> the inner film thickness could be, yet still effect the charge trapping reaction (7) at all (as opposed to direction oxidation of PVFer by the Pt electrode), and how rapidly $PVFer^+$ trapped states formed with very thin inner films leak away. Figure 10 shows a cyclic voltammogram where Γ_T for the inner film poly-$Ru(vbpy)_3^{2+}$ layer

was only 6×10^{-10} mol./cm^2 , or ca. 40 Å. The initial positive potential scan shows only a small anodic current inflection at ca. +0.44 volt vs. SSCE (the thermodynamic potential for PVFer oxidation in acetonitrile), and then a large current peak at +0.93 volt (Curve E) from previous studies we know to be the trapping reaction[1,2]. This result demonstrating charge trapping for very thin inner layers, is significant in that switching times for these film assemblies as charge rectifying or as stably switched electrochromic surfaces[5] are thereby predicted for equally thin outer films to be as short as (by the approximate thickness relation, $\sqrt{D_{ct}t}$) ca. 1 msec.

Following scanning through the poly-[Ru(vbpy)$_3$]$^{3+/2+}$ wave at +1.1 volt, no reverse wave for PVFer$^+$ reduction is seen (as expected[1,2]). If the potential is scanned again positively from zero volts immediately or after pause-waiting periods of 1, 2 or 4 minutes (Curves A-D), a retrapping peak is observed near +0.9 volts whose magnitude does not increase proportionately to the waiting time. This indicates that leakage does occur for this thin inner film but not all regions of the film leak away charge at equal rates.

The wave at ca. +0.44 volt in Figure 11is notable both for its small size and its shape. The charge under the +0.44 volt wave is $< 5\%$ of the +0.93 volt initial charge trapping peak; very little ferrocene is oxidized by permeation through the inner film poly-[Ru(vbpy)$_3$]$^{2+}$ film. That which is oxidized gives a membrane diffusion cyclic voltammetric shape reminiscent of that in Figure 9, Curve D, which implies that slow diffusion of PVFer chains into the poly-Ru(vbpy)$_3^{2+}$ polymer can occur on a time scale of a second or so. However, this polymer/polymer interpenetration does not over the course of time homogenize the films (else no trapping peak at all), so the PVFer diffusion must more resemble a large-scale polymer segment vibration than a net

diffusional mass transport. This particular observation is of interest with respect to the stability of bilayer polymer film assemblies and the kinetics of electron transfer trapping reactions at the polymer/polymer, poly-[Ru(vbpy)$_3$]$^{3+}$/PVFer interface[70].

CONCLUSIONS

This paper demonstrates the feasibility of electrochemically preparing ultrathin redox polymer films which exhibit both molecular size and charge discrimination toward solutes in contact with them. This observation is significant in that the ruthenium polymers have redox properties making them potential oxidation catalysts for electro-organic reactions; their permeability characteristics also suggest the possibility of size selective oxidation processes by the polymer, and/or by the underlying electrode or other catalyst. The discrimination of molecular size is, crudely, comparable to that of zeolitic structures[10,11].

Acknowledgement. This research was supported in part by grants from the National Science Foundation and the Office of Naval Research.

References

1. Abruña, H. D.; Denisevich, P.; Umaña, M.; Meyer, T. J.; and Murray, R. W. J. Amer. Chem. Soc. 103 (1981) 1.
2. Denisevich, P.; Willman, K. W.; and Murray, R. W. J. Amer. Chem. Soc. 103 (1981) 4727.
3. Denisevich, P; Abruña, H. D.; Leidner, C. R.; Meyer, T. J.; and Murray, R. W. Inorg. Chem., in press.
4. Schmehl, R.; and Murray, R. W., unpublished results.
5. Willman, K. W.; and Murray, J. Electroanal. Chem., in press.
6. Blank, M., Ed.; "Biochemistry: Ions, Surfaces, Membranes", Adv. Chem. Series, vol. 88, 1980.
7. Tepfer, M.; and Taylor, I. E. P. Science 213 (1981) 761.
8. Kydonieus, A. F. "Controlled Release Technologies: Methods, Theory, and Applications", vol. 1, CRC Press, 1980, pp.
9. Carr, R. W.; and Bowers, L. D. "Immobilized Enzymes In Analytical and Clinical Chemistry", John Wiley and Sons, New York, 1980.
10. Barrer, R. M. "Molecular Sieve Zeolite", Adv. Chem. Series, 102 (1971) 41.
11. Eberly, P. E. "Zeolite Chemistry and Catalysis", Rabo, J. A.; ACS Monograph Series, ACS Press, 1976, pp. 392.
12. Fendler, J. H.; and Fendler, E. J. "Catalysis in Micellar and Macromolecular Systems", Academic Press, New York, 1975.
13. Infelta, P. P.; Gratzel, M.; and Fendler, J. H. J. Amer. Chem. Soc. 102 (1980) 1479.
14. Nomura, T.; Escabi-Perez, J. R.; Sunamoto, J.; and Fendler, J. H. J. Amer. Chem. Soc. 102 (1980) 1484.

15. Oyama, N.; and Anson, F. C. Anal. Chem. 52 (1980) 1192.

16. Oyama, N.; Shigehara, K.; and Anson, F. C. Inorg. Chem. 20 (1981) 518.

17. Peerce, P. J.; and Bard, A. J. J. Electroanal. Chem. 112 (1980) 97.

18. Doblhofer, K.; Nolte, D.; and Ulstrup, J. Ber. Bunsenges. Phys. Chem. 82 (1978) 403.

19. Lacaze, P.-C.; Pham, M.-C.; Delamar, M.; and Dubois, J.-E. J. Electroanal. Chem. 108 (1980) 9.

20. Dautartas, M. F.; and Evans, J. F. J. Electroanal. Chem. 109 (1980) 301.

21. Schroeder, A. H.; and Kaufman, F. R. J. Electroanal. Chem. 113 (1980) 209.

22. Kaufman, F. B.; Schroeder, A. H.; Engler, E. M., Kramer, S. R.; and Chambers, J. Q. J. Amer. Chem. Soc. 102 (1980) 483.

23. Bettelheim, A.; Chan, R. J. H.; and Kuwana, T. J. Electroanal. Chem. 110 (1980) 93.

24. DeGrand, C.: and Laviron, E. J. Electroanal. Chem. 117 (1981) 283.

25. Oyama, N., Sato, K.; and Matsuda, H. J. Electroanal. Chem. 115 (1980) 149.

26. Samuels, G. J.; and Meyer, T. J. J. Amer. Chem. Soc. 103 (1981) 307.

27. Miller, L. L.; and Van De Mark, M. R. J. Amer. Chem. Soc. 100 (1978) 3223.

28. Miller, L. L.; and Van De Mark, M. R. J. Electroanal. Chem. 88 (1978) 437.

29. Kerr, J. B.; and Miller, L. L. J. Electroanal. Chem. 101 (1979) 263.

30. Kerr, J. B.; Miller, L. L.; and Van De Mark, M. R. J. Amer. Chem. Soc. 102 (1980) 3383.

31. DeGrand, C.; and Miller, L. L. J. Electroanal. Chem. 117 (1981) 267.

32. Kuo, K. N.; and Murray, R. W. J. Electroanal. Chem., in press.

33. Ikeda, T.; Leidner, C. R.; and Murray, R. W. J. Amer. Chem. Soc., in press.

34. Rocklin, R. D.; and Murray, R. W. J. Phys. Chem. 85 (1981) 2104.

35. Murray, R. W. Philosoph. Trans. Royal Society, London, Phil. Trans. R. Soc, Lond. A 302 (1981) 253.

36. Andrieux, C. P.; and Saveant, J.-M. J. Electroanal. Chem. 93 (1978) 163.

37. Andrieux, C. P.; Dumas-Bouchiat, J. M.; and Saveant, J.-M. J. Electroanal. Chem. 114 (1980) 159.

38. Andrieux, C. P.; and Saveant, J.-M. J. Electroanal. Chem. 111 (1980) 377.

39. Andrieux, C. P.; Dumas-Bouchiat, J. M.; and Saveant, J.-M., J. Electroanal. Chem., in press.

40. Bolts, J. M.; Bocarsly, A. B.; Palazzotto, M. C.; Walton, E. G.; Lewis, N. S.; and Wrighton, M. S. J. Amer. Chem. Soc. 101 (1979) 1378.

41. Bookbinder, D. C.; Lewis, N. S.; Bradley, M. G.; Bocarsly, A. B.; and Wrighton, M. S. J. Amer. Chem. Soc. 101 (1979) 7721.

42. Lewis, N. S.; Bocarsly, A. B.; and Wrighton, J. Phys. Chem. 84 (1980) 2033.

43. Dautartas, M. F.; Mann, K. R.; and Evans, J. F. J. Electroanal. Chem. 110 (1980) 379.

44. Anson, F. C. J. Phys. Chem. 84 (1980) 3336.

45. Peerce, P. J.; and Bard, A. J. J. Electroanal. Chem. 114 (1980) 89.

46. Schroeder, A. H.; Kaufman, F. B.; Patel, V.; and Engler, E. M. J. Electroanal. Chem. 113 (1980) 193.

47. Laviron, E. J. Electroanal. Chem. 112 (1980) 1.

48. Daum, P.; Lenhard, J. R.; Rolison, D. R.; and Murray, R. W. J. Amer. Chem. Soc. 102 (1980) 4649.

49. Nowak, R. J.; Schultz, F. A.; Umaña, M.; Lam. R.; and Murray, R. W. Anal. Chem. 52 (1980) 315.

50. Daum, P.; and Murray, R. W. J. Electroanal. Chem. 103 (1979) 289.

51. Daum, P.; and Murray, R. W. J. Phys. Chem. 85 (1981) 389.

52. Facci, J.; and Murray, R. W. J. Electroanal. Chem., 124 (1981) 339.

53. Ikeda, T.; Leidner, C. R.; and Murray, R. W., submitted.

54. Sullivan, B. P.; Salmon, D. J.; and Meyer, T. J. Inorg. Chem. 17 (1978) 3334.

55. Schilt, A. A. Inorg. Synth. 12 (1970) 247.

56. Gough, D. A.; and Leypoldt, J. K. Anal. Chem. 51 (1979) 439.

57. Bazier, M. M.; "Organic Electrochemistry", M. M. Bazier, ed., New York, Marcel Dekker, 1973, pp. 679-704.

58. a) Rubenstein, I.; J. Phys. Chem. 85 (1981) 1899;
b) Rubenstein, I.; and Bard, A. J. J. Amer. Chem. Soc. 103 (1981) 5007.

59. Kuwana, T.; Bublitz, D. E.; and Hom, G. J. Amer. Chem. Soc. 82 (1960) 5811.

60. Nicholson, R. S.; and Shain, I.; Anal. Chem. 36 (1964) 706.

61. That current density uniformity is important is shown by considerable sensitivity to the placement of the auxiliary electrode during polymerization[3].

62. Baizer, M. M.; "Organic Electrochemistry", M. M. Bazier, ed., New York, Marcel Dekker, 1973, pp. 947-975.

63. Including the boundary of the inner surface of any remaining gaps or canyons.

64. Gueshi, T.; Tokuda, K.; and Matsuda, H. J. Electroanal. Chem. 89 (1978) 247.

65. Landsberg, R.; and Thiele, R. Electrochim. Acta 11 (1966) 1243.

66. Scheller, F.; Muller, S.; Landsberg, R.; and Spitzer, H.-J. J. Electroanal. Chem. 19 (1968) 187.

67. Scheller, F.; Landsberg, R.; and Muller, S. J. Electroanal. Chem. 20 (1969) 375.

68. We observe this, since D_S determined from the reciprocal Levich plots agrees with naked electrode D_S .

69. The Levich behavior in Figure 4 (—o—) for the mediated ferrocene oxidation rxn, 5 indicates that $k_{crs}\Gamma > \sim 0.5$ cm/s., i.e., is beyond our measurable[53] limit. With the measured $PD_{S,pol} = 1.3 \times 10^{-8}$ cm^2/s. for ferrocene in Table V, the estimation of ferrocene penetration beyond the

poly-$[Ru(vbpy)_3]^{2+}$/solution interface is simply, $PD_{S,pol}/k_{crs}\Gamma >$ 2.6×10^{-8} cm., less than a monolayer dimension. The calculation for Rxn. 4 is done similarly.

70. Denisevich, P.; Willman, K.; and Murray, R. W., unpublished results.

TABLE I

CLASSES OF BEHAVIOR OBSERVED FOR SOLUTE PERMEATION THROUGH poly-$[Ru(vbpy)_3]^{2+}$ POLYMER FILMS

Rate of Solute (Reactant) Permeation	Reaction Site(s)	Waves Observed	Potential of solute reaction; diagnostic characteristics	Examples
very fast	Electrode Surface	1	Same as at naked electrode; linear Levich plot	Br^-/Br_2
very slow	Film/solution interface	1	Shifted toward polymer potential; linear Levich plot	$[Ru(bpy)_2(py)Cl]^{+1/+2}$
measurable	1. Electrode surface, and	2	1. Same as at naked electrode; linear reciprocal Levich plot	Fer/Fer^+
	2. Film/solution interface		2. Shifted toward polymer potential; linear Levich plot	

TABLE II

Permeation Rates of Various Electroactive Solutes Through Pt/poly-Ru($\underline{vbpy}$)$_3^{2+}$ Films, in 0.1 $\underline{M}$ Et_4NClO_4/CH_3CN

	Γ_T, mol./cm^2	C_S, x10^3 $\underline{M}$	Intercept, x10^{-6}, amp^{-1}	D_S, x10^5, cm^2/s.	$PD_{S,pol}$/d, cm/s.	$PD_{S,pol}C_{Ru}$, mol./cm.s.
Ferrocene						
$E^{o'}$ = +0.38V	7.2×10^{-10}	0.07	0.034	2.4	4.2×10^{-2}	3.0×10^{-11}
	7.8×10^{-10}	0.18	0.021	2.4	2.2×10^{-2}	1.7×10^{-11}
	1.1×10^{-9}	0.18	0.029	2.0	1.6×10^{-2}	1.7×10^{-11}
	1.2×10^{-9}	0.17	0.024	2.4	2.0×10^{-2}	2.4×10^{-11}
	2.5×10^{-9}	0.07	0.30[a]	-	4.6×10^{-3}	1.2×10^{-11}
	6.8×10^{-9}	0.07	0.67[a]	-	1.8×10^{-3}	1.2×10^{-11}
				D_S (at naked Pt)[b]: 2.3×19^{-5} cm^{2}s^{-1}		$1.9 \pm 0.7 \times 10^{-11}$
Benzoquinone						
$E^{o'}$ = -0.51$_5$V	7.8×10^{-10}	0.12	0.0048	2.6	1.5×10^{-1}	1.2×10^{-10}
	1.1×10^{-9}	0.12	0.0080	2.2	8.9×10^{-2}	9.8×10^{-11}
	2.0×10^{-9}	0.11	0.026	4.4	2.9×10^{-2}	5.8×10^{-11}
	3.6×10^{-9}	0.11	0.035	5.0	2.1×10^{-2}	7.6×10^{-11}
				D_S (at naked Pt): 2.2×10^{-5} cm^{2}s^{-1}		$8.7 \pm 2.1 \times 10^{-11}$
diquat^{2+}						
$E^{o'}$ = -0.37V	7.8×10^{-10}	0.19	0.078	1.2	5.6×10^{-3}	4.4×10^{-12}
	1.1×10^{-9}	0.19	0.31	1.0	1.4×10^{-3}	1.5×10^{-12}
				D_S (at naked Pt): 1.1 x 10-5 cm^{2}s^{-1}		$3.0 \pm 1.5 \times 10^{-12}$

Table II continued
page 2 of 2

$Ru(bpy)_2Cl_2$						
$E^{o'} = +0.29_5 V$	7.8×10^{-10}	0.17	0.35	1.4	1.4×10^{-3}	1.1×10^{-12}
	9.7×10^{-10}	0.04	0.82	1.1	2.5×10^{-3}	2.4×10^{-12}
	9.7×10^{-10}	0.09	0.29	0.81	3.2×10^{-3}	3.1×10^{-12}
	9.7×10^{-10}	0.15	0.19	0.84	3.0×10^{-3}	2.9×10^{-12}
	1.1×10^{-9}	0.17	0.62	0.84	7.8×10^{-4}	8.6×10^{-13}
	1.2×10^{-9}	0.12	0.33[a]	-	2.1×10^{-3}	2.5×10^{-12}
	2.1×10^{-9}	0.12	1.33[a]	-	5.2×10^{-4}	1.0×10^{-12}
			D_S (at naked Pt): $1.3 \times 10^{-5} cm^2 s^{-1}$			$2.0 \pm 0.9 \times 10^{-12}$
$Fe(bpy)_2(CN)_2$						
$E^{o'} = +0.44_5 V$	7.8×10^{-10}	0.18	0.83[a]	-	5.5×10^{-4}	4.3×10^{-13}
	1.2×10^{-9}	0.14	1.0[a]	-	5.9×10^{-4}	7.1×10^{-13}
	2.7×10^{-9}	0.32	2.0[a]	-	1.3×10^{-4}	3.5×10^{-13}
			D_S (at naked Pt): $0.87 \times 10^{-5} cm^2 s^{-1}$			$5.0 \pm 2.0 \times 10^{-13}$

a. $i_\ell \neq f(\omega^{1/2})$

b. $D_S = 2.4 \times 10^{-5}$ $cm^2 s^{-1}$ from ref. 59, 2.8×10^{-5} $cm^2 s^{-1}$ from ref. 5-9.

TABLE III

Permeation Rates of Electroactive Solutes Through Pt/poly-$[Ru(\underline{bpy})_2(\underline{p}\text{-}\underline{cinn})_2]^{2+}$ Films in 0.1 M Et_4NClO_4/CH_3CN

	Γ_T, mol./cm^2, x10^{10}	C_S, x10^3, M	D_Sx10^5, cm^{2}sec^{-1}	$PD_{S,pol}C'_{Ru}$, mol./cm.s.
$[Ru(\underline{bpy})_2Cl_2]$	4.11	0.0826	1.65	1.2×10^{-11}
	7.83	0.0826	1.51	1.5×10^{-11}
	9.68	0.0826	1.88	9.2×10^{-12}
	11.9	0.067	1.85	1.1×10^{-11}
	21.2	0.0826	-	1.7×10^{-11}
	25.0	0.10	0.45	1.5×10^{-11}
	49.6	0.067	0.99	1.4×10^{-11}
	49.6	0.10	1.05	1.1×10^{-11}
	130.0	0.10	-	1.5×10^{-11}
				Avg. $1.3_5 \times 10^{-11}$
ferrocene	15.2	0.135	2.11	12.6×10^{-11}
	23.4	0.10	1.25	8.8×10^{-11}
	28.1	0.135	1.90	17.1×10^{-11}
	46.6	0.135	2.02	13.5×10^{-11}
	55.3	0.135	1.89	11.7×10^{-11}
	58.1	0.10	1.22	8.3×10^{-11}
	75.7	0.10	1.41	10.6×10^{-11}
				Avg. 11.8×10^{-11}

TABLE IV

Permeation Rates of Electroactive Solutes Through Pt/poly-VDQ^{2+} Films in 0.1 M Et_4NClO_4/CH_3CN

	Γ_T, mol./cm^2	C_S, x10^3 M	Intercept, x10^{-6}, amp^{-1}	D_S x10^5, cm^2/s	$PD_{S,pol}/d$, cm^{2}s^{-1}	$PD_{S,pol}C_{VDQ}$ mol./cm.
Ferrocene	4.4 x 10^{-10}	0.10	0.16	2.7	5.1 x 10^{-3}	2.2 x 10^{-12}
	6.3 x 10^{-10}	0.10	0.23	1.2	3.5 x 10^{-3}	2.2 x 10^{-12}
	1.3 x 10^{-9}	0.18	0.27	1.8	2.2 x 10^{-3}	2.9 x 10^{-12}
$[Ru(bpy)_2Cl_2]$	1.3 x 10^{-9}	0.26	0.68[a]	-	6.1 x 10^{-4}	7.9 x 10^{-13}
$[Ru(bpy)_3]^{2+}$	1.3 x 10^{-9}	0.15	2.7[a]	-	2.7 x 10^{-4}	3.5 x 10^{-13}

a. $i_l \neq f(\omega^{1/2})$

TABLE V

$PD_{S,pol}$ For Various Electroactive Solutes
Through Electrochemically Polymerized Films[a]

$PD_{S,pol}$ through:	poly-$[Ru(vbpy)_3]^{2+}$[b]	poly-$[Ru(bpy)_2(p\text{-}cinn)_2]^{2+}$[c]	poly-VDQ^{2+}[d]
Solute			
bromide	$> 4 \times 10^{-7}$		
p-benzoquinone	5.8×10^{-8}		
ferrocene	1.3×10^{-8}	9.0×10^{-8}	1.0×10^{-9}
$[Ru(\underline{bpy})_2Cl_2]$	1.3×10^{-9}	1.0×10^{-8}	3.3×10^{-10}
$[Fe(\underline{bpy})_2(CN)_2]$	3.3×10^{-10}		
$diquat^{2+}$	2.0×10^{-9}		
$[Ru(\underline{bpy})_2(\underline{py})Cl]^{+}$	$< 7 \times 10^{-12}$		
$[Ru(\underline{bpy})_3]^{2+}$			1.5×10^{-10}

a. Assuming maximum redox site concentrations as in footnotes b, c, d, for unswollen films.

b. $C_{Ru} = 1.5 \times 10^{-3}$ mol./cm^3 based on 1.35 g./cm^3 density[3].

c. $C_{Ru} = 1.3 \times 10^{-3}$ mol./cm^3 based on 1.40 g./cm^2 density.

d. $C_{VDQ} = 2.4 \times 10^{-3}$ mol./cm^3 based on assumed unity density.

FIGURE LEGENDS

Figure 1. Cyclic voltammetry at 0.1 v/s of $Ru^{III/II}$ reaction for Pt/poly-$[Ru(\underline{vbpy})_3]^{2+}$ (Curve A) and Pt/poly-$[Ru(\underline{bpy})_2(\underline{p\text{-}cinn})_2]^{2+}$ (Curve B) electrodes in 0.1 M Et_4NClO_4/CH_3CN. Γ_T = 5.8 x 10^{-9} and 5.3 x 10^{-9} mol./cm^2, respectively.

Figure 2. Rotated Pt/poly-$[Ru(\underline{vbpy})_3]^{2+}$ (Γ_T = 3.6 x 10^{-9}mol./cm^2) disk voltammetry in 0.1 M Et_4NClO_4/CH_3CN. No added bromide (Curve A); 0.1- mM Bu_4NBr (Curve B). v = 0.02 v/s, S = 77 $\mu A/cm^2$, ω = 6400 rpm. Inset is limiting current measured at 0.95 v. as a function of $\omega^{1/2}$.

Figure 3. Rotated disk voltammograms of 0.20 mM $[Ru(\underline{bpy})_2(\underline{py})Cl]^+$ in 0.1 M Et_4NClO_4/CH_3CN at naked Pt (Curve A) and Pt/poly$[Ru(\underline{vbpy})_3]^{2+}$ (Γ_T = 7.8 x 10^{-10} mol./cm^2) (Curve B) electrodes. v = 0.02 v/s, S = 77 $\mu a/cm^2$, ω = 6400 rpm. Figure insets are Levich plots of limiting currents of Curve A (-x-) and Curve B (-o-) and 10X scale expansion (S = 7.7 $\mu a/cm^2$) of foot of Curve B.

Figure 4. Rotated disk voltammograms of 0.070 mM ferrocene in 0.1 M Et_4NClO_4/CH_3CN at Pt/poly-$Ru(vbpy)_3^{2+}$ (Γ_T = 7.2 x 10^{-10} mol./cm^2) (Curves A - D, electrode rotation rate 400, 1600, 3600, and 6400 rpm, respectively), and naked Pt (Curve E, 6400 rpm). v = 0.02 v/s, S = 19 $\mu a/cm^2$. Figure inset is limiting currents of ferrocene at naked Pt (-●-) and at Pt/poly-$Ru(vbpy)_3^{2+}$ for permeation wave (-x-) measured at 0.6 volt and mediated wave (-o-) measured at 1.1 volt.

Figure 5. Reciprocal Levich plots for permeation wave for ferrocene oxidation at Pt/poly-$Ru(vbpy)_3^{2+}$. Curve A - C: C_S = 0.070, 0.18, 0.18 mM; $\Gamma_T = 7.2 \times 10^{-10}$, 1.1×10^{-9} , 7.8×10^{-10} mol./cm^2, respectively.

Figure 6. Rotated disk voltammogram at 0.17 mM $[Ru(bpy)_2Cl_2]$ in 0.1 M Et_4NClO_4/CH_3CN at naked Pt (Curve A) and (Curve B) Pt/poly-$[Ru(vbpy)_3]^{2+}$ ($\Gamma_T = 7.8 \times 10^{-10}$ mol./cm^2) electrodes. v = 0.02 v/s, S = 77 μa/cm^2, ω = 6400 rpm. Inset is limiting currents measured at (–x–) 0.5 volt on Curve A and at (–●–) 0.5 volt and (–o–) 1.1 volt on Curve B.

Figure 7. Rotated disk voltammograms of 0.19 mM $diquat^{2+}$ in 0.1 M Et_4NClO_4/CH_3CN at naked Pt (Curve A) and Pt/poly-$[Ru(vbpy)_3]^{2+}$ ($\Gamma_T = 7.8 \times 10^{-10}$ mol./cm^2) electrodes. v = 0.02 V/s, S = 39 μa/cm^2, ω = 6400 rpm. Figure inset is reciprocal Levich plot for limiting currents of Curve B (Line 1) and of another example where $\Gamma_T = 1.1 \times 10^{-9}$ mol./cm^2 (Line 2).

Figure 8. PD_S/d from reciprocal Levich plot intercepts are inversely proportional to Γ_T , film thickness. Results for ferrocene (x) and $[Ru(bpy)_2Cl_2]$ (o) in poly-$[Ru(vbpy)_3]^{2+}$ (– – –) and for ferrocene (●) and $[Ru(bpy)_2Cl_2]$ (△) in poly-$[Ru(bpy)_2(p\text{-}cinn)_2]^{2+}$ (——).

Figure 9. Rotated disk voltammetry of 0.1 mM ferrocene in 0.1 M Et_4NClO_4/CH_3CN at naked Pt (Curve A) and Pt/poly-VDQ^{2+} ($\Gamma_T = 6.3 \times 10^{-10}$ mol./cm^2). v = 0.02 v/s, S = 19 μa/cm^2, ω = 3600 rpm. Stationary electrode cyclic voltammetry for naked Pt (Curve C) and Pt/poly-VDQ^{2+} (Curve D)

Figure 9 continued:

in same solution at 0.1 v/s.

Figure 10. Cyclic voltammetry (0.1 v/s) of a Pt/poly-Ru($\underline{vbpy}$)$_3$]$^{2+}$/PVFer bilayer electrode were Γ_{inner} is 6 x 10^{-10} mol./cm^2 . Curve E: virgin scan 0 → +1.6 → 0 volt; Curve A: immediately repeated scan; Curves B - D repeated after 1, 2, 4 minute pause at 0 volt, respectively. Charges under trapping peaks are (Curves A - E), 1.6 x 10^{-10}, 3.8 x 10^{-10} , 6.2 x 10^{-10} , 8.9 x 10^{-10} , 2.5 x 10^{-9} mol./cm^2.

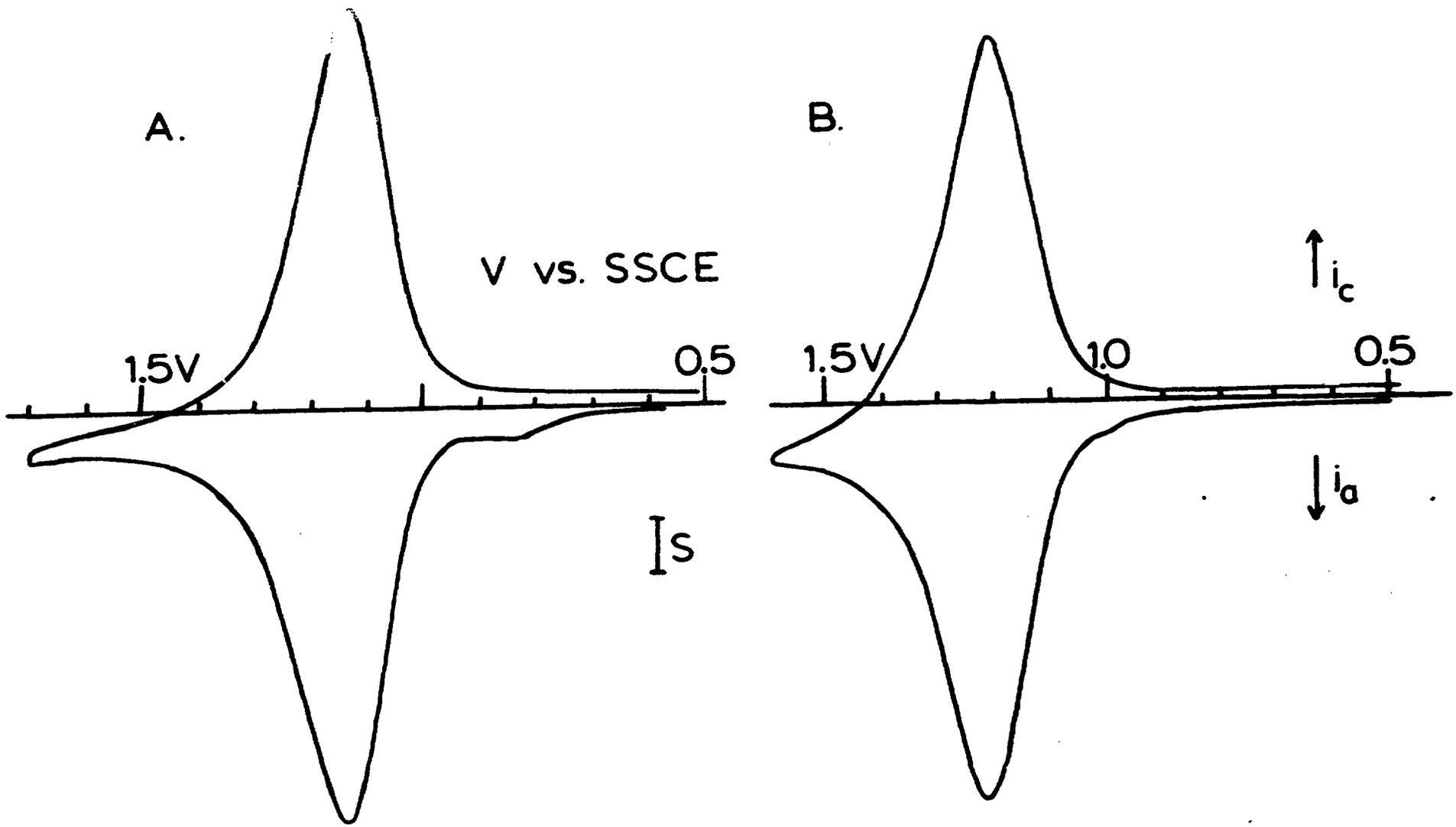
A.
V vs. SSCE
1.5V
0.5
Is
B.
i_c
1.5V
1.0
0.5
i_a

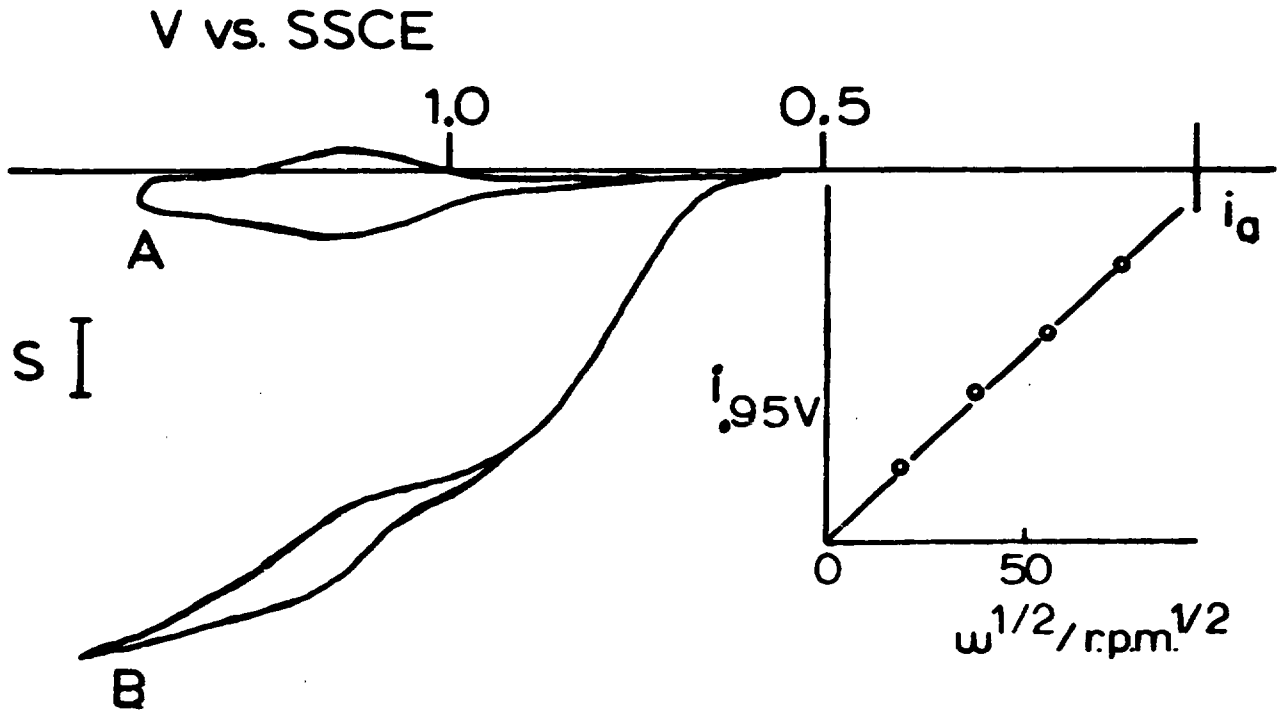
V vs. SSCE
1.0
0.5
A
B
S
i_a
$i_{.95V}$
0
50
$\omega^{1/2}$/r.p.m.$^{1/2}$

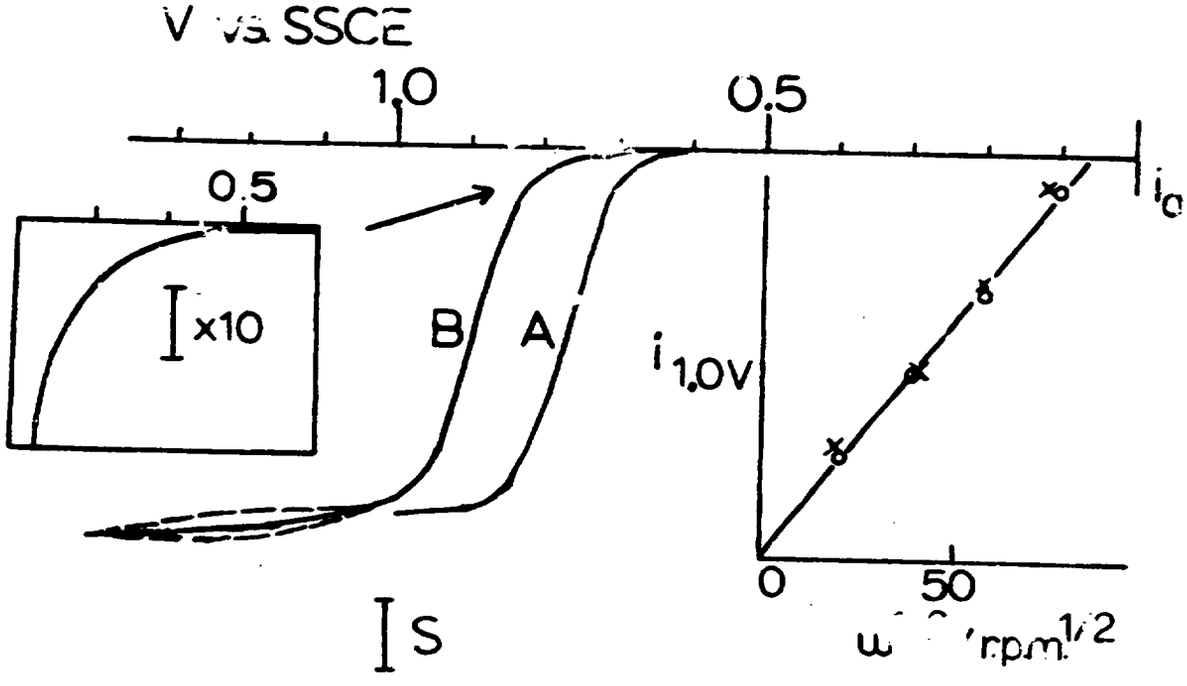
V vs SSCE
1.0
0.5
0.5
I x10
B
A
$i_{1.0V}$
i_d
0
50
$\omega^{1/2}$ rpm$^{1/2}$
I S

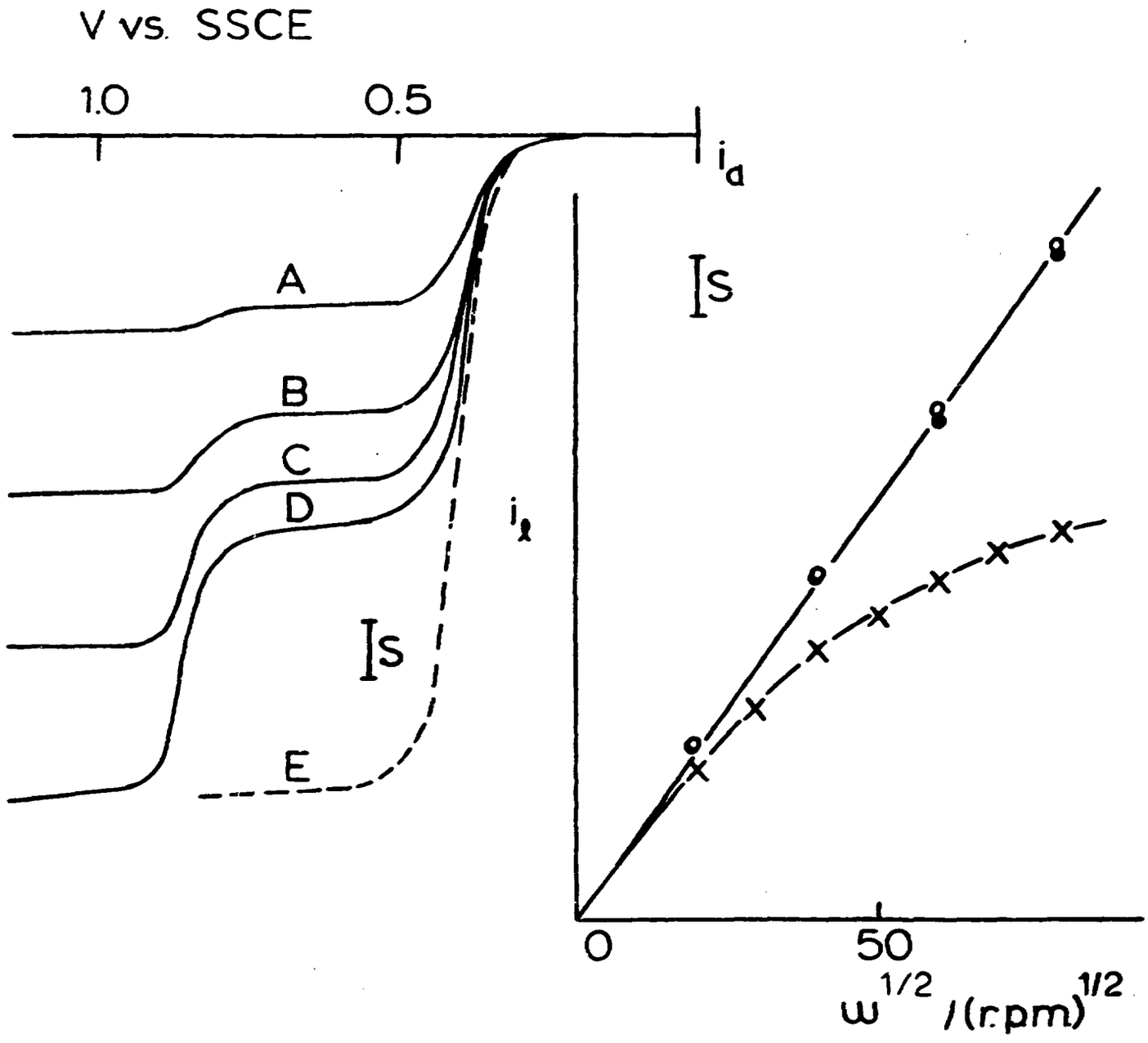
V vs. SSCE
1.0
0.5
i_d
A
B
C
D
E
I_S
i_l
I_S
0
50
$\omega^{1/2}$ /(r.p.m)$^{1/2}$

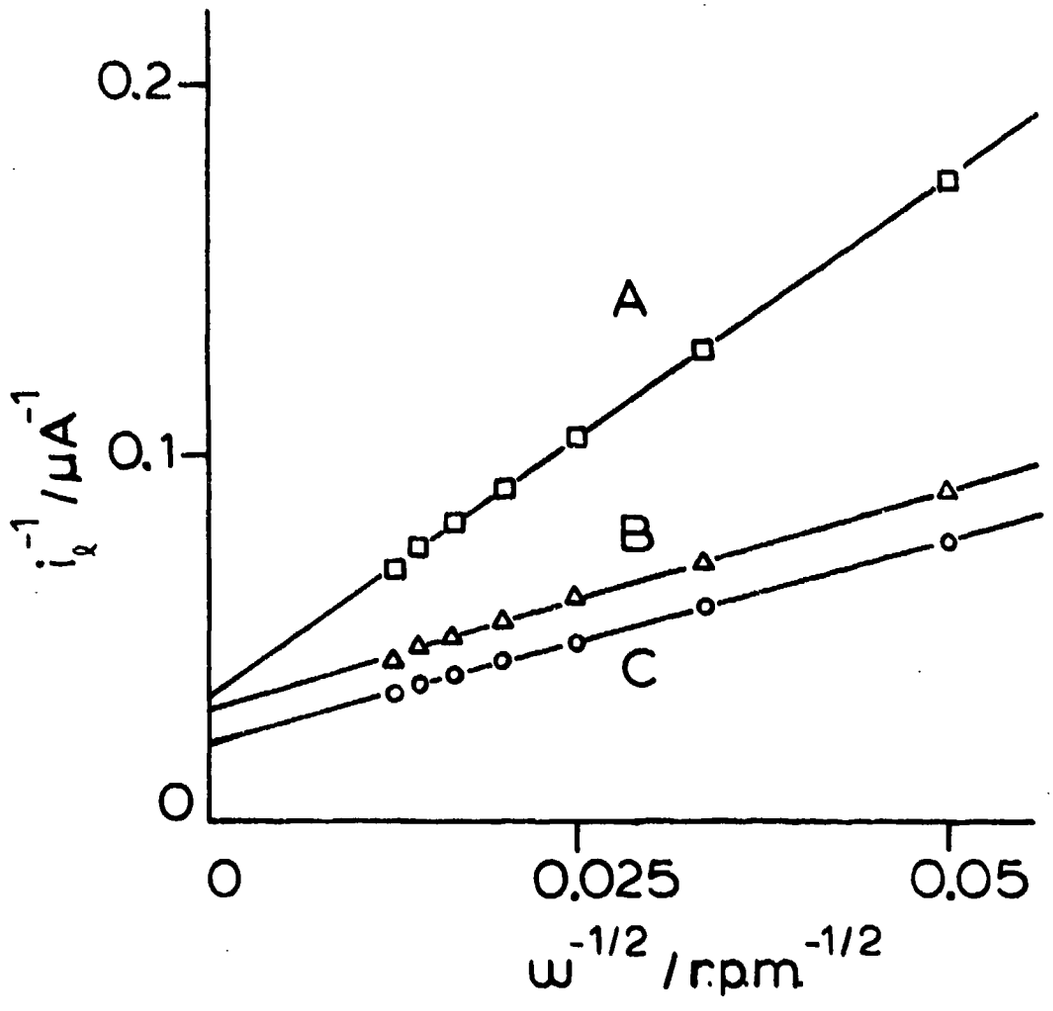
0.2
0.1
0
i_l^{-1} /μA^{-1}
A
B
C
0
0.025
0.05
$\omega^{-1/2}$ /r.p.m.$^{-1/2}$

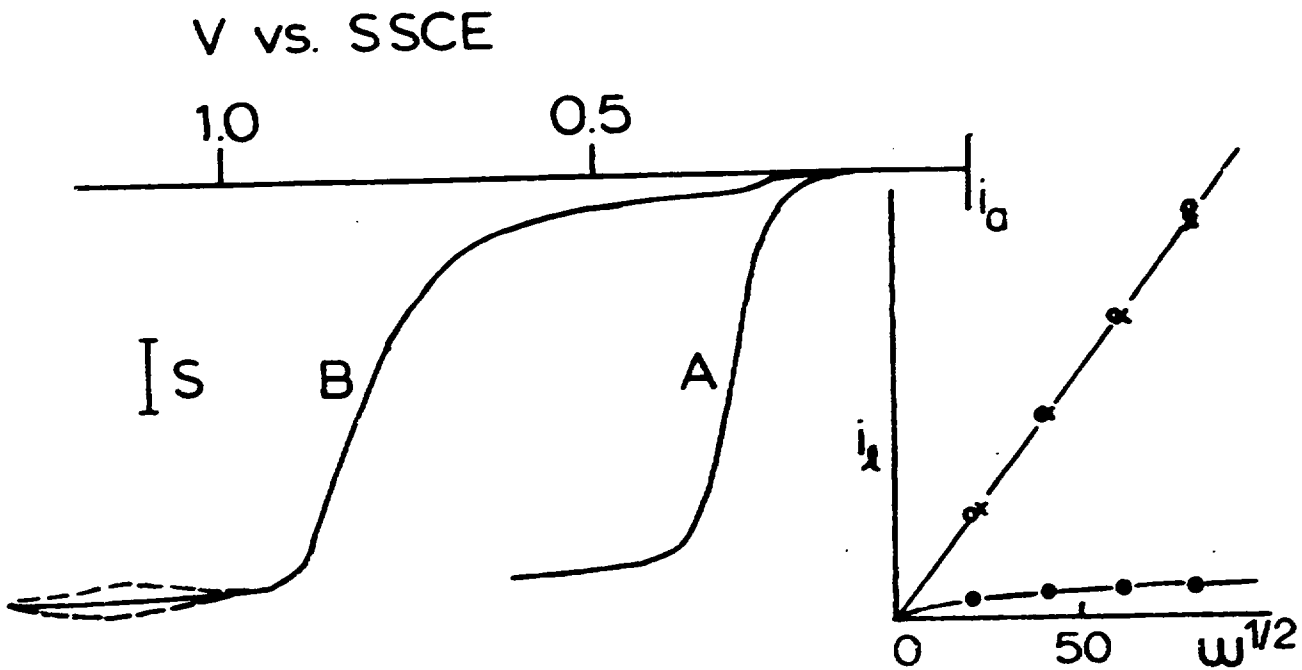
V vs. SSCE
1.0
0.5
i_a
I_S
B
A
i_l
0
50
$\omega^{1/2}$

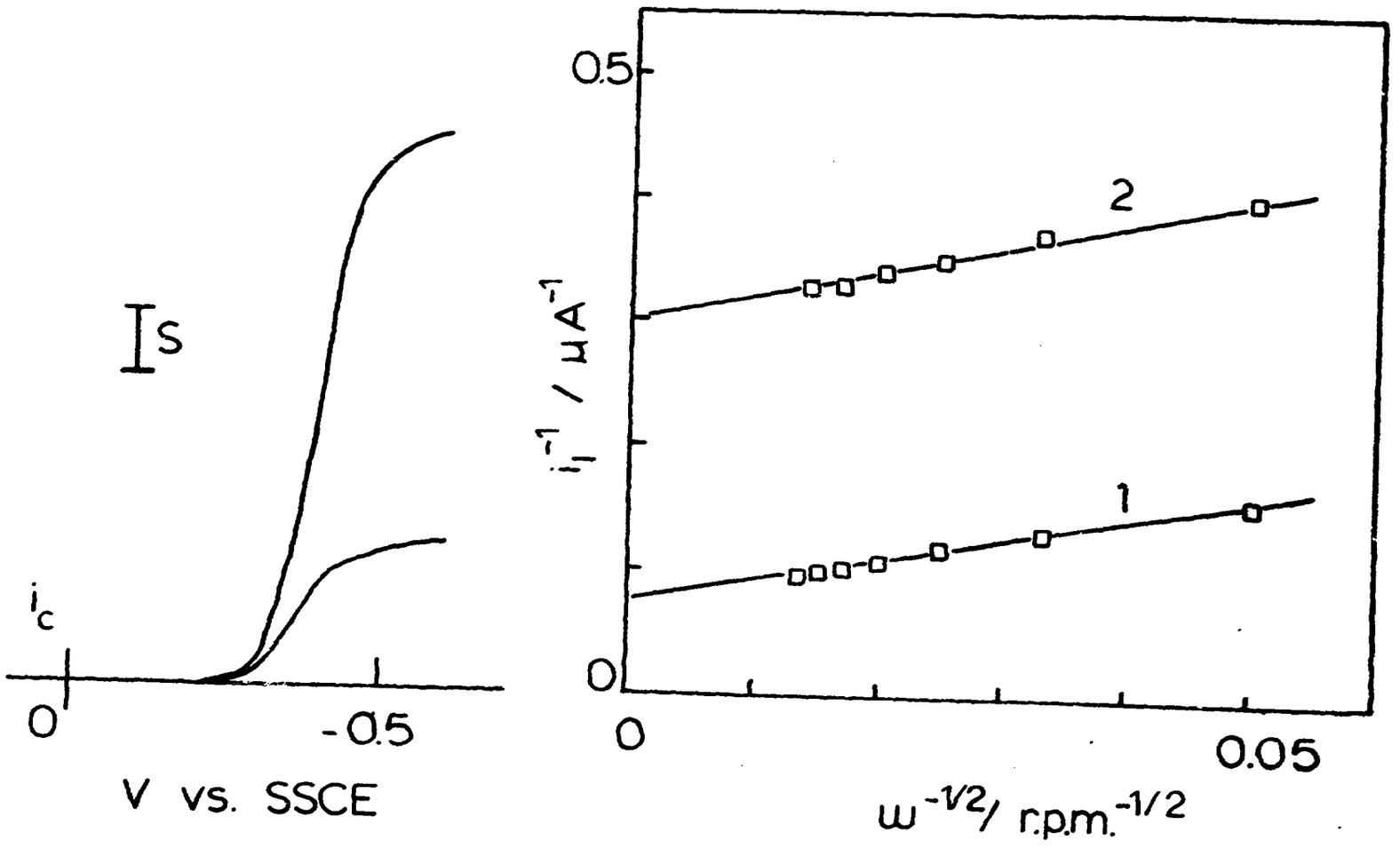
Is
i_c
0
-0.5
V vs. SSCE
0.5
0
i_l^{-1} / μA^{-1}
2
1
0
0.05
$w^{-1/2}$/ r.p.m.$^{-1/2}$

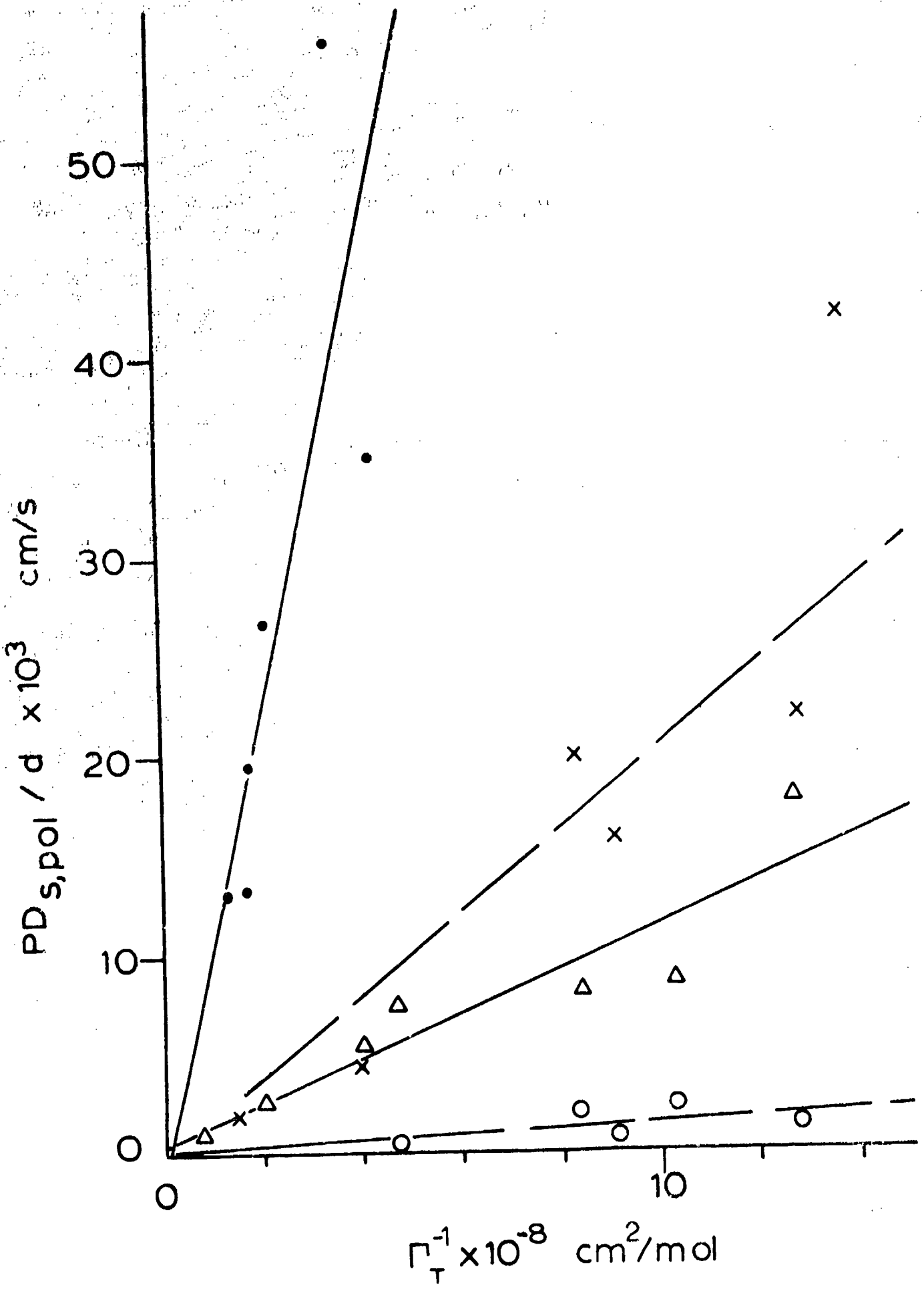
50
40
30
20
10
0
0
10
$PD_{s,pol} / d \times 10^3$ cm/s
$\Gamma_T^{-1} \times 10^{-8}$ cm^2/mol

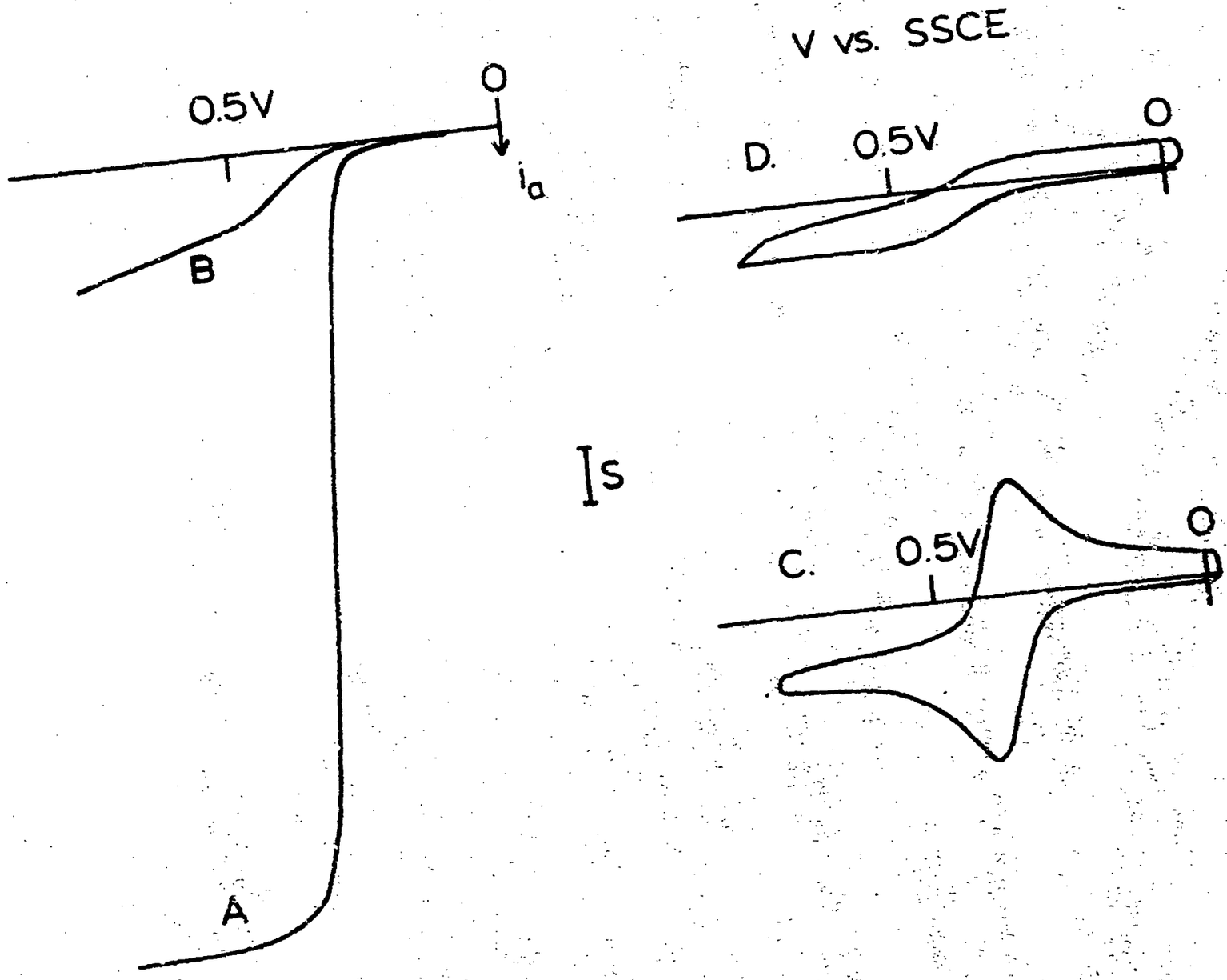
V vs. SSCE
0.5V
O
i_a
B
A
I_S
D.
0.5V
O
C.
0.5V
O

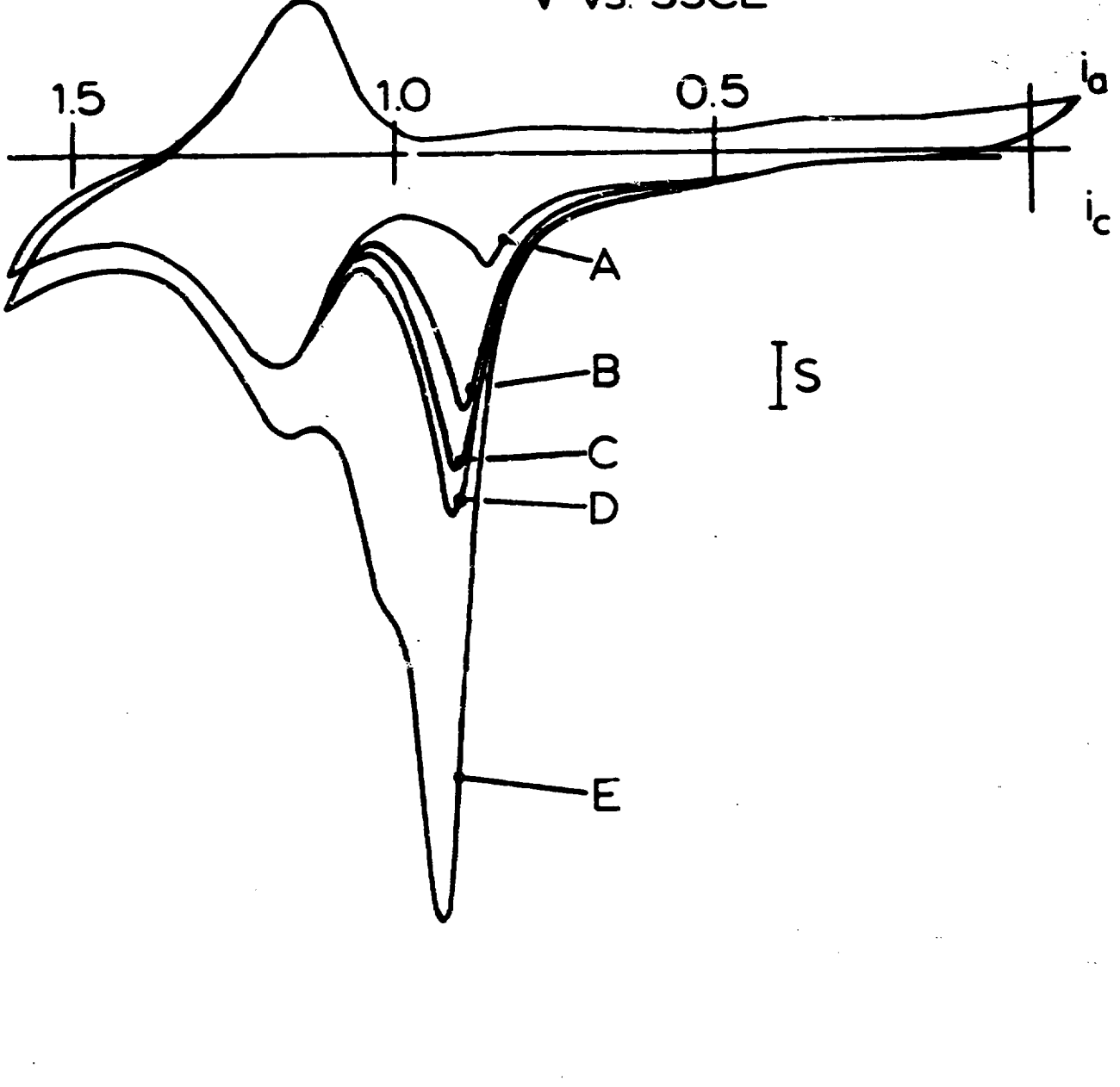
V vs. SSCE
1.5
1.0
0.5
i_a
i_c
A
B
C
D
E
I_S